



# Archeomagnetic intensity investigations of French medieval ceramic workshops: Contribution to regional field modeling and archeointensity-based dating

Agnès Genevey, Yves Gallet, Erwan Thébault, Philip W. Livermore, Alexandre Fournier, Sébastien Jesset, Annie Lefèvre, Nadine Mahé-Hourlier, Emmanuel Marot, Stéphane Regnard

## ► To cite this version:

Agnès Genevey, Yves Gallet, Erwan Thébault, Philip W. Livermore, Alexandre Fournier, et al.. Archeomagnetic intensity investigations of French medieval ceramic workshops: Contribution to regional field modeling and archeointensity-based dating. *Physics of the Earth and Planetary Interiors*, 2021, 318, pp.106750. 10.1016/j.pepi.2021.106750 . hal-03284542

**HAL Id: hal-03284542**

**<https://hal.science/hal-03284542>**

Submitted on 8 Nov 2021

**HAL** is a multi-disciplinary open access archive for the deposit and dissemination of scientific research documents, whether they are published or not. The documents may come from teaching and research institutions in France or abroad, or from public or private research centers.

L'archive ouverte pluridisciplinaire **HAL**, est destinée au dépôt et à la diffusion de documents scientifiques de niveau recherche, publiés ou non, émanant des établissements d'enseignement et de recherche français ou étrangers, des laboratoires publics ou privés.



Distributed under a Creative Commons Attribution - NonCommercial - NoDerivatives 4.0 International License

**Archeomagnetic intensity investigations of French Medieval ceramic workshops:  
Contribution to regional field modeling and archeointensity-based dating**

**A. Genevey<sup>1</sup>, Y. Gallet<sup>2</sup>, E. Thébault<sup>3</sup>, P. W. Livermore<sup>4</sup>, A. Fournier<sup>2</sup>, S. Jesset<sup>5</sup>, A. Lefèvre<sup>6</sup>, N. Mahé-Hourlier<sup>7</sup>, E. Marot<sup>8</sup>, S. Regnard<sup>9</sup>**

*<sup>1</sup>Sorbonne Université, CNRS, Laboratoire d'Archéologie Moléculaire et Structurale, LAMS, F-75005 Paris, France*

*<sup>2</sup>Université de Paris, Institut de Physique du Globe de Paris, CNRS, F-75005 Paris, France*

*<sup>3</sup>Université Clermont Auvergne, CNRS, IRD, OPGC, Laboratoire Magmas et Volcans, F-63000 Clermont-Ferrand, France*

*<sup>4</sup>School of Earth & Environment, University of Leeds, Leeds, UK*

*<sup>5</sup>Pôle d'Archéologie Ville d'Orléans, F-45000 Orléans, France*

*<sup>6</sup>Institut national de recherches archéologiques préventives, Centre de recherches archéologiques de la Courneuve, F-93126 La Courneuve, France*

*<sup>7</sup>Institut national de recherches archéologiques préventives, Centre de recherches archéologiques de Passy, F-89510 Passy, France*

*<sup>8</sup>Bourges Plus, Service d'archéologie préventive, F-18000 Bourges, France*

*<sup>9</sup>Centre de recherches archéologiques du Vexin français, F-95450 Guiry-en-Vexin, France*

**Keywords**

Archeointensity, Medieval period, Western Europe, Field intensity modeling, Archeointensity dating

## Highlights

- 7 new Triaxe archeointensity data are obtained from French medieval pottery workshops
- They allow a refinement of the evolution of intensities during the High Middle Ages
- A set of available intensity data is re-examined based on cooling rate correction
- We illustrate the sensitivity of regional intensity models to modeling strategies
- We discuss two different procedures for archeointensity dating

## Abstract

Seven new archeointensity data are obtained through the analysis of groups of pottery and kiln fragments from ceramic workshops unearthed in France, precisely dated from the High Middle Ages. The measurements are carried out using the Triaxe magnetometer, following a dedicated experimental protocol that takes into account the effects of anisotropy and cooling rate (CR) on thermoremanent magnetization acquisition. The new data are consistent with the evolution of intensity variations described by our previous data obtained in France and Northern Italy, which display between the 5<sup>th</sup> and 10<sup>th</sup> c. a pronounced camel-back shape. In particular, they provide supporting evidence of an intensity minimum that occurred around the transition between the 7<sup>th</sup> and 8<sup>th</sup> century. These data, combined with a selection of previously published results within a 700 km radius of Beaune and re-examined based on CR correction, formed the basis of new regional mean intensity variation curves based on two independent modeling approaches. The first algorithm developed by Thébault and Gallet (2010) based on bootstrapping and now irregularly spaced knots according to the data distribution gives rather smooth intensity variations, while the second approach proposed by Livermore et al (2018) based on a transdimensional Bayesian technique shows more abrupt variations with sometimes stronger amplitudes. We explore the dating potential of these two

variations curves, which have an unprecedented resolution, by studying two medieval pottery workshops. Six fragment groups (three per workshop) are analyzed using the Triaxe protocol, providing mean archeointensity values for each of the two sites. Two different procedures are used for their dating, either by comparing the intensity value to be dated with the reference intensity variation curves obtained from the two modeling techniques or by analyzing the marginal posterior probability distribution of the age values derived from the method of Livermore et al (2018). For France, the two techniques yield very similar results. The archeointensity dating results combined with archeological arguments and radiocarbon data, make it possible to better constrain the age of the end of activity of the two workshops. Archeointensity investigation of displaced materials thus appears as an effective means to obtain original chronological constraints on the age of their production, paving the way for a wide range of complementary research on Medieval pottery.

## **1. Introduction**

Archeomagnetism is a method now commonly implemented in the field of archeology throughout the European area to provide chronological constraints on fired clay artifacts whose dating requires refinement. This tool is based on the use of local reference curves of the temporal variations of the geomagnetic field in direction and/or intensity, either directly obtained from the analysis of numerous dated structures in the region of interest, or, when not available, deduced from regional or even global time-dependent geomagnetic field models. In Europe, one may rely on the regional SCHA-DIF.4K field model covering the past four millennia recently constructed by Pavón-Carrasco et al. (2021), which updates and extends the previous SCHA-DIF.3K model (Pavón-Carrasco et al. 2009). The following studies indicate the breadth of existing research and interests in a variety of European countries: Belgium, Ech-Chakrouni et al. (2013); Bulgaria, Herries et al. (2008); England, Batt et al.



(2017); France, Gallet et al. (2009) and Hervé and Lanos (2017); Austria, Schnepp et al. (2015); Greece, Aidona et al. (2017); Italy, Tema et al. (2014) and Principe et al. (2018); Spain, Gómez-Paccard and Beamud (2008) and Catanzariti et al. (2007).

In France, archeomagnetism is so well integrated into the archeological fabric that this method is now included in the prescription files of preventive (rescue) excavations when heating structures are detected in situ at the time of archeological diagnosis prior to excavation. In the archeomagnetic laboratory founded in the 1930s by Emile Thellier in Saint-Maur, for instance, several hundred pottery and domestic kilns have been studied since the early 1990s, and the results used for dating purposes based on the reference directional variation curve available for the past two millennia (i.e. Thellier, 1981, Bucur, 1994, Gallet et al. 2002, Le Goff et al., 2002; 2020 in this volume).

Compared to in-situ burnt structures, the materials discovered displaced from the location where they were fired have been much less investigated archeomagnetically, in particular with the purpose of providing chronological constraints. However, archeomagnetic studies of large ensembles of architectural bricks or tiles have made it possible to refine the age of buildings from the inclination information (e.g. Lanos, 2019). On the other hand, the possibility of using the archeointensity as the only dating element for displaced objects has not yet been really exploited (Gallet et al., 2014a; Shaar et al., 2020). There are two main reasons for this: firstly, intensity data have long remained much less numerous than directional data and knowledge of intensity variations was thus very fragmentary. Secondly, and despite significant progress in intensity data acquisition all over Europe, the available data often show a dispersion that de facto limits their application for dating. A recent study by Casas and Tema (2019) explored the dating potential in Europe of the SCHA-DIF.3K model and highlighted the low added value of intensity measurements for dating. France, however, benefits from a relatively dense archeointensity dataset covering the past 1600 years, showing

little dispersion (Genevey et al., 2009; 2013; 2016; 2019). These results describe smooth millennial-scale variations punctuated by a pseudo-periodic (~260 years) succession of intensity peaks of roughly the same amplitude and each lasting ~200 years (Genevey et al., 2016; Livermore et al., 2018). Maxima are observed at the beginning of the 7<sup>th</sup> c., during the 9<sup>th</sup> c., the 12<sup>th</sup> c., at the end of the 14<sup>th</sup> c. and at the beginning of the 17<sup>th</sup> century. Genevey et al. (2016) suggested that this recurrence in intensity peaks could be related to a wave motion at the top of the core, for example due to stable stratification (see discussion in, e.g., Buffett et al., 2016). Although the reality of these peaks seems now well established, their description needs to be improved through the acquisition of new data. A densification of the archeointensity database is therefore still required, with the same effort being made for the archeomagnetic directions (see for instance Le Goff et al., 2020 in this volume).

With this objective, we present seven new Medieval archeointensity results obtained from the analysis of precisely dated groups of pottery and kiln fragments. These results allow a refinement of the reference intensity variation curve available in France. We then explore the potential of this curve for dating purposes through the study of two ceramic production sites of the High Middle Ages located in the Centre and Ile-de-France regions. The construction of the reference curve of geomagnetic field intensities and archeomagnetic dating are both carried out using two different techniques (Thébault and Gallet, 2010; Livermore et al., 2018), which allows us to compare them and to illustrate the implications of selecting one single regional modeling and/or dating option rather than the other.

## **2. Description of the collected archeological fragments.**

### **2.1 Dated ceramic sets**

Among the new groups of fragments, five come from two ceramic production areas largely exploited in our previous intensity studies i.e. Saran in the Centre region of France and

Vanves located close to Paris, in the Ile de France region (Fig. 1a). At Saran, the analysis of groups SAR19 and SAR21 completes the archeointensity study of the material from the excavation zone known as La Guignace (Bouillon, 2015). Another group (SAR36) is associated with a small production unit known as “la voie nouvelle”, which was discovered more recently and dated from the first half of the 7<sup>th</sup> century (Jeset, to be published). The two groups from Vanves, referred to as VAN03 and VAN09, come from the excavations conducted in Rue Gaudray (Lefèvre and Peixoto, 2015), from which some materials were already studied for archeointensity (Gallet et al. 2009; Genevey et al. 2016). The VAN03 group has been re-sampled with fragments taken from almost complete pots isolated by A. Lefèvre because they have a morphology typical of the production of the associated kiln. The numbering of the fragments from this group thus starts at number 23 (Supp. Table1). The dating of these five groups is mainly based on typo-chronological constraints previously described in Genevey et al. (2016). For that reason, we exclusively collected fragments of pottery lips whose shape is clearly identified and characteristic of the production.

The other groups are associated with two ceramic production sites recently unearthed and both located in the Ile-de-France region, at Hermé (c. 85 km south-east of Paris) and Chamigny (c. 60 km east of Paris, Fig. 1a). The rescue excavations at the site known as “Hermé Les Malletons (S.P.M. carrière)” were carried out in 2014 by the French National Institute for Preventive Archeological Research (INRAP), being motivated by the establishment of a new quarry. These excavations revealed a discontinuous occupation of the site from Prehistory to the beginning of the 11<sup>th</sup> c. (Chaudriller, 2019). Focusing on the High Middle Ages period, the site was a rural settlement during the 7<sup>th</sup> c. with a husbandry activity. Towards the middle of the 9<sup>th</sup> c. the site evolved and two types of workshop were developed, linked to metallurgical and ceramic productions. Four pottery kilns document this later activity. Three phases of production were evidenced: during the second half of the 9<sup>th</sup> c., at

the beginning of the 10<sup>th</sup> c., and finally around the end of the 10th century. Only the last two phases were sampled for archeointensity analysis. Three groups of ceramic fragments (called HERME01 to HERME03) are respectively associated with the productions of kilns F1621 and F3160 of the intermediate phase (beginning of the 10<sup>th</sup> c.) and with kiln F3060 of the last phase (end of the 10<sup>th</sup> c.). Unfortunately, none of these pottery fragments provided archeointensity results (*infra.*). For the last phase, we doubled the sampling with a group of fragments collected from Kiln 3060 (HERME04). The fragments were taken all along the central tongue support of the kiln particularly well preserved and made of limestone covered with a thin clay layer (Fig. 1b). The potsherds that were found inside the kiln show a clear rupture with respect to the previous productions of the site, whether it concerns the profile, the edge, or the handle of the pots. Based on the form of the pottery, all fragments were dated prior to the end of the 10<sup>th</sup> century and a dating between c. 970 and 1000 is thus retained for the last activity of the kiln (and thus for the HERME04 group). It should be noted that archeomagnetic dating based on directions was conducted on the same kiln (N. Warmé in Chaudriller, 2019). A 95%-confidence level dating between 900 and 1080 was obtained using the new reference curve determined by Le Goff et al. (2020 in this volume). Within this time window, the interval [940-990] appears however as being the most probable with a maximum probability c. 960 (see description of the method in Le Goff et al., 2002), which is in good agreement with the ceramological constraints.

At Chamigny, the excavations at the place called "la grande maison" are recent, carried out in the summer of 2017. Conducted by INRAP, they were prescribed following a project for the construction of individual houses. Two distinct occupation phases have been observed on this site: The first is dated to the Neolithic period, then, after a long period of abandonment, a re-occupation is documented from the end of the 6<sup>th</sup>-early 7<sup>th</sup> c. until the end of the 10<sup>th</sup> century (Mahé, 2020). It is mainly characterized by metallurgical and pottery

activities. Several groups of fragments from the different pottery production units (five kilns in total) were sampled for archeointensity measurements but only one group (CHAM03) has provided successful results so far. This group consists of fragments from the working area of kiln 2629 (Fig. 1c). The dating of this production is constrained by morphological and stylistic elements given by the numerous fragments found inside the kiln. Among other elements, one may mention the absence of carinated bowls, the importance of deep shapes with short collar and re-entrant rim or jugs with a shamrock-shaped tubular spout. They indicate a dating around the end of the 7<sup>th</sup> c. - very beginning of the 8<sup>th</sup> century (Mahé, 2020).

## **2.2 Sets of ceramics collected in order to provide chronological constraints**

The first site studied was excavated during the fall-winter of 2015-2016 by the archeological service of the urban community of the city of Bourges (in the center of France, Fig. 1a). These excavations were carried out before the construction of a housing estate in the city La Chapelle Saint Ursin (Bourges's suburbs) at the place called "l'angoulaire, chemin des vallées aux fruscades" (Marot, 2017). This site mainly revealed the existence of a Roman villa constructed *ex nihilo* at the beginning of the 1<sup>st</sup> century AD. The villa remained in activity until the 6<sup>th</sup> c. with successive modifications and enlargements. The last phase saw the installation of a small ceramic production unit for the inhabitants of the villa and surrounding area. The objective of our work was to provide chronological constraints about the end of this pottery activity. To this purpose, we sampled fragments of pottery characteristic of the production found in the kiln, as well as fragments of the kiln itself. For the pottery, two groups were collected corresponding to pottery wasters showing deformations for the first set (BOUR01), and evidence of overfiring for the second (BOUR02). The samples from the kiln itself correspond to fired clay fragments from the dome that were found in the filling

(BOUR03). It may be stressed that no archeomagnetic directional study was carried out at the time of the excavations.

The second site was excavated in 1997 after the fortuitous discovery of a burial site on private land in Vienne-en-Arthies in the hamlet of Chaudry (50 km northwest of Paris, Fig. 1a). The excavations, made over a small area, were entrusted to the Centre de Recherches Archéologiques du Vexin Français (CRAVF; Regnard 1999). They revealed the existence of a pottery kiln of which only the heating chamber was unearthed (the rest of the kiln being located outside the excavated area). It was filled by a largely standardized ceramic production of pots for cooking, with a mainly sandy and, to a lesser extent, granular paste. This site is the only witness currently known of a production in the Vexin Français region (Fig. 1a: area in yellow) during the Carolingian period, although archeologists presume the existence of a more important pottery production in this region. Three groups of potsherds were selected with the objective of better constraining the period of activity of this pottery production, especially its end. The first two groups consist of fragments with a grey sandy paste (CHAU01) and grey-brown sandy paste (CHAU02) which are typical of this production, while the last group comprises fragments with red granular re-baked paste (CHAU03). These later potsherds were most probably used for the construction of the kiln. We note that this kiln, only partially excavated, was not sampled for archeomagnetic directional analysis.

### **3. Measurements workflow**

The workflow in this study is identical in all respects to the one used in our previous archeointensity studies conducted on Western European artifacts (Genevey et al. 2009, 2013, 2016, 2019). All experiments were carried out at the paleomagnetic laboratory of the Institut de Physique du Globe de Paris (IPGP).

The evolution of magnetic susceptibility in weak field was first measured for each fragment during heating-cooling cycles between room temperature and c. 500°C. These measurements were performed using an Agico Kappabridge KLY3-S coupled with a CS3 furnace. The reversibility of the susceptibility curves, evaluated visually, allowed the selection of the fragments that are *a priori* most favorable for intensity measurements (carried out over the same temperature range).

For each fragment, a first specimen was then measured for intensity determination using the Triaxe protocol. If the observed behavior met our quality criteria or was promising for intensity determination, other specimens were then measured. This is also the case if the chosen temperature range was not adequate for the first specimen. The Triaxe experimental method and our quality criteria have been extensively detailed in previous publications (e.g. Le Goff and Gallet, 2004, Gallet and Le Goff, 2006, Genevey et al., 2009, Hartmann et al., 2010, Gallet et al. 2014b) and recently by Troyano et al. (2021 in this volume). We remind the reader that the magnetization measurements are performed automatically at high temperatures following a protocol that takes into account the anisotropy and cooling rate effects on thermoremanent remanent magnetization (TRM) acquisition, and minimizes possible effect related to the presence of multidomain grains (Genevey et al., 2009, Hartmann et al., 2010; 2011, Hervé et al., 2017, Shaar et al., 2020). As for the quality criteria, they aim to test the stability on heating of the magnetic mineralogy (thanks in particular to magnetic susceptibility vs. temperature curves), the quality of the individual determination and the consistency of the results both at the fragment (with a minimum of two specimens per fragment and an error between them of less than 5%) and fragment group levels. A minimum of three fragments successfully analyzed per group and an error on the mean intensity value of less than 10% and 5μT are required. The purpose of the 5%-coherence test is to exclude fragments for which we can suspect a reliability problem in the recording of the geomagnetic

signal. At the site level, our quality criteria aim mainly at assessing the temporal homogeneity of the fragments forming a group.

After the archeointensity experiments, a fragment from each retained group was subjected to Lowrie's (1990) test to provide further constraints on the magnetic mineralogy of the archeological collection. The three orthogonal IRM were acquired in a field of 1.5T, 0.4T and 0.2T using a pulse magnetometer MMPM10.

#### **4. Results**

We analyzed 157 ceramic shards and two groups of kiln fragments. Applying our quality criteria, three groups (SAR19, SAR21 and HERME04) yield a reasonable success rate between 50% and 60%. For the rest of the collection, the rate is lower, ranging between 16% and 36%, the lowest percentages being obtained for the groups studied for dating (i.e. BOUR# and CHAU#). It should be noted that these rates were calculated in relation to the number of fragments actually measured on the Triaxe. Several fragments were indeed too weakly magnetized ( $< \sim 30 \cdot 10^{-8} \text{ Am}^2$ ) with respect to the sensitivity of this magnetometer (Supp. Table 1).

The mean intensity values obtained for the different groups of fragments are reported in Table 1. Here the groups BOUR01 and BOUR02 on one hand, and CHAU01 and CHAU02 on the other hand have been merged for the computation of a mean value as these pairs are representative of the same pottery production. The eleven mean values hence determined are well defined with a maximum standard deviation of  $2.9 \mu\text{T}$  (or 3.9% of the corresponding mean; BOUR01/02 group). The consistency of the intensity results for each group of fragments is further shown in Figure 2, which presents the data at the specimen level obtained for six different groups of pottery (SAR36, CHAM03, BOUR01/02 and CHAU01/02) and kiln fragments (HERME04; BOUR03). Concerning the BOUR03 group, which consists of



fired clay fragments from the kiln dome, significant variations in colour were observed at the fragment scale, from bright red, to wine-red and brown. Of the 33 specimens tested, only the browns provided suitable results. For HERME04, the 30 specimens analyzed were taken exclusively from the limestone part of the fragments. The thin clay layer was indeed too weakly magnetized to allow analyses using the Triaxe. Such weak magnetization appears to be a characteristic of the majority of the potsherds collected at Hermé. Other shards from this site were further discarded due to strong alteration detected during the magnetic susceptibility measurements with the consequence, as previously mentioned, that no intensity results were obtained for the Hermé pottery production.

The alteration of the magnetic mineralogy revealed by the non-reversibility between the heating and cooling magnetic susceptibility curves is one of the reasons for the exclusion of several fragments (Figs. 3a,b). In almost equal proportions (i.e., 16% versus 14%), fragments were also discarded when it was impossible to isolate reliably their primary magnetization component. This is illustrated in Figure 3c where the thermal demagnetization of specimen CHAU01-10A reveals two magnetization components with widely overlapping unblocking temperature spectra, which prevented the ancient TRM from being clearly isolated. In the intensity diagram, this results in complex evolutions in the  $R'(Ti)$  data between  $T1$  (or  $T1'$ ) and  $T2$ , with significantly varying values (Fig. 3d). In general, however, most failures in intensity determination at the specimen level (70%) are related to “non-ideal” Triaxe behavior, as defined by our quality criteria, observed in the intensity diagrams, i.e., with non-constant  $R'(Ti)$  ratios over the temperature range where the primary magnetization is isolated. Specimen HERM04-08A illustrates this problem with a single component demagnetized between 150°C to 520°C (Fig. 3e) while decreasing  $R'(Ti)$  ratios are observed over the same temperature range (Fig. 3f). In rare other cases, the  $R'(Ti)$  ratios have a concave shape, also leading to the rejection of the specimen.

The thermal demagnetization of the 3-axis IRMs (recall that one fragment among those successfully analyzed was chosen for each group) shows a very classical magnetic mineralogy for baked clay artifacts (Fig. 4). The latter is first characterized by the predominance of low coercivity minerals (less than 0.2 T) with unblocking temperatures of less than 600 °C. These minerals are likely from the magnetite family with a different level of impurities. The thermal demagnetization of the hard component (1.25 T) also indicates the presence in various proportions of a high-coercivity magnetic phase with unblocking temperatures lower than 200-250 °C. These properties are compatible with those of the epsilon iron oxide, which is widespread in the materials analyzed in archeomagnetism (e.g. Chauvin et al. 2000; Hartmann et al. 2011; Genevey et al. 2016; López-Sánchez et al. 2017; 2020 in this volume). Note that the presence of hematite is not clearly attested in our collection. Finally, Figure 4 shows several examples of magnetic susceptibility vs temperatures curves. Although these measurements do not provide additional information on the magnetic mineralogy (since the heating is only conducted up to 500-520 °C), they illustrate the reversibility criterion applied on magnetic susceptibilities which is taken into account in our archeomagnetic studies.

## **5. Selection of data available within a 700 km radius of Beaune with a focus on the cooling rate effect**

Our seven precisely-dated new results are reported in Figure 5 together with our previous data obtained mainly in France, but also in Belgium (for one datum) and more recently in Tuscany in northern Italy. As in our last publication, all data have been reduced to the common site of Beaune in Burgundy (47.02°N, 4.84°E). At this stage, we observe that the new results are consistent with the intensity variations described from our previous datasets which display between the 5<sup>th</sup> and 10<sup>th</sup> c. a pronounced camel-back shape (Genevey et al., 2016). They make

it possible to better define the hump that occurred during the 7<sup>th</sup> and 8<sup>th</sup> c., with a maximum reached around 600 AD followed by a decrease until the beginning of the 8<sup>th</sup> century. Moreover, Hermé's result dating from the end of the 10<sup>th</sup> c. helps to trace more precisely the strong and remarkable decrease in intensities, by  $\sim 20 \mu\text{T}$ , which occurred between the beginning of the 9<sup>th</sup> c. and the end of the 10<sup>th</sup> century.

Other archeointensity results dating from the past 1700 years were previously obtained within the 700 km-radius of Beaune. As in our previous publications, these data were examined through a set of selection criteria, retaining only those obtained using Thellier and Thellier (1959) derived protocols including at least two pTRM-checks or with the Shaw (1974) method. The number of intensity results used to derive the mean is required to be greater or equal to three and the errors around the mean value must be of less than 15% (this threshold is therefore less restrictive than the one used for our own data). The TRM anisotropy must also be taken into account when objects more sensitive to this effect are analyzed (such as pottery or tiles). An additional criterion concerns the age uncertainties, which must be less than or equal to  $\pm 50$  years. Applying these criteria, the remaining dataset comprises results obtained by Chauvin et al. (2000) and Gómez-Paccard et al. (2012) with respectively seven and four data from France, Casas et al. (2005) (one English result), Donadini et al. (2008) and Donadini et al. (2012) with respectively one and two data from Switzerland, and Schnepf et al. (2020 in this volume) with four data from Germany. Eleven of these data were derived from the study of in-situ burnt structures, i.e., kilns or fireplaces, with analyzed samples from bricks (five data) and baked clay (five data), while baked rocks were collected in one case. The eight other results were obtained from the analysis of artifacts discovered displaced from the location where they were produced: bricks in seven cases and tiles in the last one.

348       The cooling rate (CR) effect is another parameter whose importance has been  
349       discussed in several studies (for a general discussion see Brown et al. (2021) in this volume,  
350       but also Genevey et al. 2003, 2008, Hervé et al., 2019; Kostadinova-Avramova and  
351       Jordanova, 2019; Jones-Cervantes et al., 2020). With regard to the correction of this effect,  
352       different strategies were implemented for the 19 data above. In particular, it was not  
353       considered by Casas et al. (2005), whereas it was evaluated for each analyzed fragment by  
354       Chauvin et al. (2000). The mean values per group of fragments were then computed using  
355       only CR-corrected data. The situation is more complex for the other studies. For the data  
356       obtained by Gómez-Paccard et al. (2012), the CR effect is evaluated for each fragment but a  
357       correction is applied only when the percentage of alteration is lower than the percentage of  
358       CR correction. We recall that the alteration percentage is calculated from a loop-back test  
359       identical to a pTRM-check. It allows us to ascertain the stability of the magnetic mineralogy  
360       from measurements specifically dedicated to the evaluation of the CR effect. The average per  
361       group of fragments was then calculated combining both uncorrected and CR-corrected  
362       intensity determinations. The values concerned are reported in Supplementary Figure 1. For  
363       the result obtained at Angers, the majority of the values (86%) were CR-corrected and the  
364       general mean calculated by Gómez-Paccard et al. (2012) ( $81.3 \pm 10.8 \mu\text{T}$ ) is consistent with the  
365       average obtained using only the CR-corrected data ( $82.7 \pm 11.3 \mu\text{T}$ ). For the other three groups,  
366       only 33 to 38% of the collection were CR-corrected, leading to three different situations. For  
367       the Mont-Saint-Michel site, the CR-corrected values show the same distribution as the  
368       uncorrected ones (supp. Fig. 1). Therefore, the mean value calculated with all the data or with  
369       only the CR-corrected data is fairly similar ( $69.9 \pm 7.0 \mu\text{T}$  versus  $70.0 \pm 7.4 \mu\text{T}$ ). At Pierrefitte-  
370       sur-Sauldre, the CR-corrected data are in the middle of the distribution of all the values (supp.  
371       Fig. 1), and the mean calculated using only these data ( $83.6 \pm 1.1 \mu\text{T}$ ) presents an error much  
372       smaller but within the uncertainty interval of the mean derived from all data ( $89.3 \pm 8.7 \mu\text{T}$ ).

Finally, for the fragment group at Saran, the CR-corrected values are all much lower than the uncorrected ones (supp. Fig. 1). The mean obtained from the CR-corrected values has a smaller error ( $67.8 \pm 3.6 \mu\text{T}$ ) but, above all, it is not compatible with the average calculated using all the data ( $79.9 \pm 8.3 \mu\text{T}$ ). It is interesting to note that this group corresponds to fragments from a kiln sampled at Saran, whose filling has already been analyzed by Genevey et al. (2016) (A36/SAR08 group) who found a mean intensity of  $72.0 \pm 3.6 \mu\text{T}$ . Genevey et al. (2016) proposed a possible time gap between the last use of the kiln and its filling to explain the difference between the results, although there is no archeological evidence to support this option. Considering only the CR-corrected data obtained by Gómez-Paccard et al. (2012) now leads to a mean intensity value ( $67.8 \pm 3.6 \mu\text{T}$ ) compatible with that of Genevey et al. (2016). It thus appears that the strategy used by Gómez-Paccard and co-authors is not adequate in certain circumstances, in particular when the distributions of the CR-corrected and non-corrected values are different. Below, for the results of Gómez-Paccard et al. (2012), we chose to retain only the mean values computed using the CR-corrected data.

We also analyzed in more detail the result obtained by Donadini et al. (2008). Here again the situation is different with fragments from the same medieval kiln analyzed both in the paleomagnetic laboratory at Helsinki and Sofia. At Helsinki, small (volume  $1 \text{ cm}^3$ ) and larger (volume  $8 \text{ cm}^3$ ) samples were measured, and a fan was used for cooling the fragments during the Thellier experiments. At Sofia, only large samples (volume  $8 \text{ cm}^3$ ) were studied and the oven used for the Thellier experiments was left cooled without a fan. As expected, the mini-samples systematically gave higher values (Supp. Fig. 1). An arbitrary decrease of 10% accounting for the CR effect was thus applied to those data by Donadini et al. (2008), which *de facto* reduced the difference with the other results, but still with higher values (Supp. Fig. 1). The mean intensity value for this medieval kiln was computed by combining the data from the large samples (Helsinki and Sofia) without changes and those from the mini samples

corrected by 10%. This leads to a mean value with a small error ( $86.85 \pm 1.49 \mu\text{T}$ ) which likely does not express the real uncertainties associated with this determination. We have preferred to keep only the results from the Sofia analyses (large samples, no fan,  $83.9 \pm 3.9 \mu\text{T}$ ), assuming they are less affected by the CR effect although a residual CR effect is possible.

The next set of two data was acquired by Donadini et al. (2012) from Medieval fireplaces unearthed in Zurich. The sample's volume is  $8 \text{ cm}^3$ , therefore corresponding to that of the big samples in the 2008 study (i.e. those for which no CR correction was applied). No CR experiment was performed; instead, an educated-guess decrease of 10% was applied to both data. Given the uncertainty about the relevance of this arbitrary correction, we have preferred not to retain these two values.

The last data set recently acquired by Schnepf et al. (2020) includes four data obtained by the Thellier method, in its original version or in the version modified by Coe (1967), but only three of them were CR-corrected, with an experimental evaluation of this effect for each specimen. We therefore retained these three data, while the fourth result for which the CR-effect was not explored was discarded. For the same reason, we also did not retain the result of Casas et al. (2005). In our region of interest, Schnepf et al. (2020) also obtained several intensity results using the multi-specimen method (Biggin and Poidras, 2006; Dekkers and Böhm, 2006) according to the so-called MSP-DSC technique developed by Fabian and Leonhardt (2010). Without prejudging their reliability nor consistency with the other data, we chose at this stage not to consider them because the CR-effect on the multi-specimen results would still deserve further investigation (Schnepf et al., 2020).

This leaves us with the original dataset of Chauvin et al. (2000), four mean results from the Gómez-Paccard et al. (2012) study calculated using only the CR-corrected data, one result from Donadini et al. (2008) derived from the analysis of big samples at Sofia laboratory where no fan was used and the three CR-corrected data from Schnepf et al. (2020 in this

volume). These twelve data are reported in Figure 5. They are all consistent with our own dataset (e.g., Genevey et al., 2019), thus entering in the same evolutionary trend, albeit often showing either higher or lower intensity values.

## **6. Construction of a secular variation curve**

In our previous studies focused on the field intensity variations in Western Europe over the past 1600 years, we successively applied two modeling strategies to derive a mean variation curve. Genevey et al. (2013; 2016) used the approach developed by Thébault and Gallet (2010) based on an iteratively reweighted least-squares inverse technique combined with a bootstrap algorithm exploring the intensity and dating uncertainties of each data point. It allows the computation of a large set of individual models using cubic B-splines whose knots are evenly spaced, according to the average of the time intervals between data. The time interval between two knots was equal to 70 years in Genevey et al. (2013) and 50 years in Genevey et al. (2016). A master curve is then provided in the form of probability density function (pdf) as a function of time. One of the objectives of this approach is to reduce the effects of possible outliers. This is achieved thanks to the use of Huber weights for the experimental data errors, the latter being normally distributed within one standard deviation and less steeped beyond, and a re-weighted least-squares scheme. An important point is that the algorithm now includes uneven knot positions, according to the temporal distribution of the data, which allows us to provide a more robust and detailed determination of the intensity field variations.

More recently, Genevey et al. (2019) used the transdimensional Bayesian method developed by Livermore et al. (2018), which is based on piecewise linear regression of the available data. The number and temporal distribution of the linear segments are imposed by the data according to their experimental and dating uncertainties, without a priori hypothesis

on the complexity of the intensity variations to be determined (i.e. with a minimum level of regularization). A perturbation procedure called AH-RJMCMC (for Age Hyperparameter - Reverse Jump Monte Carlo Markov Chain; see explanations in Livermore et al., 2018) allows the determination of a large ensemble of models whose distribution (pdf), mean, median, mode and 95% credible interval are provided, as well as the posterior intensity and age distributions of each individual datum (Livermore et al., 2018, 2021 in this volume; see also Lanos, 2004; Hellio and Gillet, 2014; Hervé and Lanos, 2017). All calculations are made using a wide prior distribution of the intensity values for each knot common to two consecutive segments, which has been here chosen between 35  $\mu$ T and 95  $\mu$ T; the maximum number of knots over the entire documented time interval is conservatively set to 150. Finally, it should be noted that both techniques allow us to take into account a possible time-order relationship between subsets of the data.

The two approaches above were used to calculate the intensity variations within the 700 km-radius of the city of Beaune in France. The computations are carried out using either our own dataset alone (Figs. 6a,c; supp. Table 2), which has the advantage of being very homogeneous from an experimental point of view, or our data combined with those described in Section 5 (Figs. 6b,d; supp. Table 2), the latter being modified along the lines discussed in this section. A good agreement is observed between the different variation curves displayed in Figure 6, which all show the same evolution mainly characterized by a series of century-scale intensity maxima. Such an agreement is not surprising given the density of the data and their overall good consistency. In detail, however, some differences are observed which are intimately linked to the methods used for the computations.

Firstly, the intensity variations are smooth when derived from the Thébault and Gallet (2010) method which considers a certain level of regularization and for which each model is constructed using cubic-B-splines, whereas the use of linear segments in the case of the



method developed by Livermore et al. (2018) gives more abrupt variations. Secondly, the pdf calculated from the two datasets using the Thébault and Gallet (2010) algorithm are fairly similar, which is expected as they differ by the addition of only twelve results. It is also worth recalling that the bootstrap algorithm tends to attenuate the effect of deviant results, and thus to determine the most robust intensity variations. Conversely, in the method developed by Livermore et al. (2018), a single result can have a significant effect on the pdf, especially if its uncertainty is small. This is well illustrated by a result at the 6<sup>th</sup>/7<sup>th</sup> c. transition obtained by Gómez-Paccard et al. (2012), with quite small experimental (1.1 $\mu$ T) and dating (65 years) uncertainties, which is higher in intensity than the other data available in the same period. When incorporated in the calculations (compare Figs. 6c and 6d), it significantly increases the amplitude of the intensity peak, whereas its effect is very minor with the Thébault and Gallet (2010) method (compare Figs. 6a and 6b). Similarly, three results obtained by Chauvin et al. (2000) between the end of the 14<sup>th</sup> c. and the first half of the 15<sup>th</sup> c. appear higher than the other data documenting this period, while one result from Schnepp et al. (2020) dated to the middle of the 13<sup>th</sup> c. is significantly lower. Here again, the incorporation of these data in the computations based on the bootstrap algorithm has little effect on the pdf (Figs. 6a,b). On the other hand, these results significantly modify the pdf obtained from the AH-RJMCMC method (compare Fig. 6c and 6d). When the data are not taken into account in the calculations (Fig. 6c), the mode of the pdf shows a linear evolution between ~1000 and ~1500, while two intensity peaks during the 11<sup>th</sup> c. and the 14<sup>th</sup> c. are only inferred from the medians, averages (the latter are not shown in Figs. 6c,d) and shape of the 95% confidence intervals of the pdf, which thus leads to rather ambiguous information. When they are taken into account (Fig. 6d), the modes of the pdf then become similar to the medians and the averages, showing the same two intensity peaks that are clearly displayed by the method of Thébault and Gallet (2010) whatever the dataset used (Figs. 6a, b).

The example above highlights the fact that a small amount of data can have a significant influence on the statistics of the models derived from the method developed by Livermore et al. (2018), in particular over a time interval wider than that strictly covered by these data. In addition, it should be noted that the 95% credible intervals provided by the AH-RJMCMC method are often wider than those given by the Thébault and Gallet (2010) method (see in particular between c. late 10<sup>th</sup> c. and early 13<sup>th</sup> c.), and the individual models are more dispersed inside the credible interval. This comes from two reasons. One arises from the AH-RJMCMC method because of the large a priori intensity range considered in the calculations, which allows for the possibility of fast and ample variations not necessarily seen from the data distribution. The second reason is that the bootstrap approach, on the contrary, uses a regularization defined as the best trade-off between the minimum complexity and the data misfit that reduces the probability of rapid and large variations in the absence of constraints provided by the data. In this way, the philosophy conveyed by the AH-RJMCMC method is very suitable to the detection of very rapid or extreme intensity variations (in this case, each result can have a strong influence on the field intensity evolution; Livermore et al., 2021 in this volume). Indeed, the method admits all possible time-dependence consistent with both the prior information and the dataset, although it returns a higher probability for parsimonious models with the least number of knots.

## **7. Contributions and limitations of archeointensity dating: case study of Bourges and Chaudry workshops**

Two procedures were used to derive chronological constraints based on archeointensity results, and also considering the reference curves established from the two different modeling techniques described in section 6 (Thébault and Gallet, 2010; Livermore et al., 2018). The first method, classical in archeomagnetism (e.g. Pavón-Carrasco et al., 2011) which we refer

below as “archeointensity correlation dating”, consists in convolving the pdf of the geomagnetic intensities defining the reference curve with the pdf of the intensity to be dated (i.e. a Gaussian) to form a (normalized) pdf of the age. It should be noted that the true pdf of the reference curves were used in our study and not, for simplification, a series of Gaussian distributions (e.g. Pavón-Carrasco et al., 2011). In this case, the intensity value to be dated is independent of the data used to create the reference curve. The second dating method, referred to as “archeointensity marginalized dating”, was described by Livermore et al (2018) and already used by Gallet et al (2020) and Shaar et al. (2020). Here, in contrast to the first method, the archeointensity value (of a priori poorly known age) to be dated is included in the dataset that constrains the joint age-intensity posterior distribution. The dating is then determined by the posterior age probability distribution derived for this datum by marginalization using the AH-RJMCMC method (see also Schnepf et al., 2015; Hervé and Lanos, 2017). The age distribution of the datum is then constrained by not only its wide prior age interval, but also by the ages of other data which are close in age. For age distributions derived either from the correlation or marginalization methods, we construct the most likely age intervals by calculating the highest density region at a 95.4% threshold (e.g. solid blue filled region in Fig 7). We will see below that the two dating methods give very similar results when using the AH-RJMCMC approach.

## **7.1 Pottery workshop of La Chapelle Saint Ursin (BOUR# groups)**

The sampling of fragments associated with the pottery kiln and its production was carried out after an initial ceramological overview. At this moment, it was possible to isolate fragments of lips associated with pots characteristic of the production. The chronological constraints on the period of activity of this small workshop were, however, still rather loose. The objective

of our study was therefore to see whether archeointensity analyses could help to better define the period of production, which was perceived as being linked to the 5<sup>th</sup> century.

The two mean intensity values obtained for the pottery (BOUR01/02) and kiln (BOUR03) fragments are very consistent (Table 1), indicating that the pottery wasters found in the kiln filling are most likely associated with the kiln's latest productions. All the results obtained at the fragment level were therefore used to calculate a mean intensity value, which should be characteristic of the ambient field that prevailed at the time the kiln was abandoned (Table 1). The overall mean intensity value was compared to the different intensity variation curves shown in Figure 6, and the results of the archeointensity correlation dating are provided in the first two columns of Table 2. While two age intervals are discriminated during the High Middle Ages with the curves constructed according to the AH-RJMCMC method (Fig. 7a), a single age interval encompassing almost the entire High Medieval Period is isolated using the curves derived from the Thébault and Gallet (2010) approach (Fig. 8a). The fact that the variation curves are respectively (for the two regional field modeling methods) more or less smooth and more or less sensitive to a very small number of data easily explain these differences (see discussion in Section 6). Furthermore, when using the AH-RJMCMC method, one can see the significant effect on the dating results induced by the choice of the database used to build the models, which is much less the case with the method of Thébault and Gallet (2010) (Table 2). On the other hand, the marginal posterior age distribution of the intensity value to be dated derived from the approach developed by Livermore et al 2018 (i.e., the archeointensity marginalized dating method; last two columns in Table 2; Fig. 7b) gives almost the same dating results as those provided by the archeointensity correlation dating method. Such an agreement can be understood by the fact that the French database is quite dense and the data very coherent, so that the incorporation of a single data point with a wide dating interval (here of 800 years between 400 and 1200) does not have much influence on

the calculated models. At this stage, it is fair to say that the results of archeointensity dating indicate that the production of this small workshop may have persisted beyond the 5<sup>th</sup> century.

This possibility was independently confirmed by the complete study of the ceramic material, which now places the production between 450 and 550, and by radiocarbon dating (Fig. 8b). The ceramic dating was first based on the study of the material "out of production" for which was noted the absence of characteristic elements of the 4<sup>th</sup> c. and early 5<sup>th</sup> c., and of Merovingian décor with a "molette" (i.e. made by impression with a wood wheel). The kiln production, with a very limited repertoire, also echoes other ensembles discovered in occupation contexts dating from the second half of the 4<sup>th</sup> c. and the first half of the 5<sup>th</sup> century. The radiocarbon dating was carried out on charcoal found in a layer associated with the last use of the kiln and should therefore be relevant for dating the end of the production. It gave an uncalibrated age of  $1580 \pm 30$  BP (Lyon-13108 (RICH)) and a calibrated age between 420 and 556 calAD (using OxCal 4.4 and IntCal20, Reimer et al. 2020).

These different dating elements, archeology, archeomagnetism (archeointensity correlation dating) and radiocarbon, can be combined to better constrain this production. Since the three dating techniques are independent, the product of their pdf is applied, yielding an age interval during the first half of the 6<sup>th</sup> c. (Fig. 8), whatever the intensity variations curves used or the method considered for deriving the archeomagnetic age intervals. Note that the radiocarbon data contributes little to this dating: combining the radiocarbon data with either the archeological or archeointensity constraints gives an age interval identical or not significantly different from that provided by archeology. In contrast, the archeointensity result in combination with the archeological constraints makes it possible to limit the age interval for the end of the pottery production to ~half a century, which brings a strong constraint for the age of abandonment of the Roman villa associated with this pottery workshop.

## 7.2 Pottery workshop of Chaudry (CHAU# groups)

The archeointensity study was carried out as part of an archeological project aimed at completely re-examining the ceramic material unearthed on this site in the late 1990s (Regnard et al. 2021). Since its discovery, this material has been recognized as dating from the Carolingian period (mid 8<sup>th</sup>-end 10<sup>th</sup> century). The re-examination of the material allowed us to detail the production, highlighting in particular the highly standardized nature of the shapes, most of which are closed, and to define several technical groups, the most significant of which have been sampled for archeointensity analyses. The objective was therefore to better define the end of the period of activity of this kiln, certainly associated with a pottery activity extending over a wider spatial area.

The two technical groups associated with the kiln's production (CHAU01/02) yielded very consistent intensity values. The results obtained from two shards (of eleven measured) used in the construction of the kiln (third technical group; group CHAU03) appeared also very close to those obtained for the CHAU01/02 group, and their incorporation does not change the mean, nor its precision (CHAU01/02:  $77.3 \pm 0.5$  versus CHAU01/02/03:  $77.4 \pm 0.4 \mu\text{T}$ ). For the archeomagnetic dating, we used the mean intensity value calculated from the data obtained for the three Chaudry groups, thus assuming that the fragments of CHAU03 were completely refired during the last use of the kiln. The archeointensity dating results obtained from this value are reported in Table 2. We find the same characteristics as before: while a single (long) age interval is obtained by correlation dating using the field evolution given by the Thébault and Gallet (2010) method (Fig. 9a), despite the very low (rather unusual) value of the standard deviation of the archeointensity data point, several distinct intervals (up to three) are observed from the AH-RJMCMC technique. For the latter, this is the case either by performing a correlation dating or by analyzing the marginal

posterior age distribution of this data point (Supp. Fig. 2), again with a significant effect of the database used on the results (Table 2).

The age interval provided by the archeological constraints is rather large, as it encompasses the entire Carolingian period (Fig. 9b). However, based on the recognition of certain regional stylistic elements, Lefèvre and Mahé (2004) proposed to narrow the production period to the first decades of the 10<sup>th</sup> century. All the results of archeointensity dating imply that the production would not have persisted beyond the very beginning of the 10<sup>th</sup> century. To test whether this observation is related to the very small standard deviation (0.4 $\mu$ T), we increased its value to 1.5 $\mu$ T. This leads to the same conclusion for the 10<sup>th</sup> century (Table 2).

Radiocarbon data from charcoal are also available for the kiln (uncalibrated age, 1255 $\pm$ 30 BP giving a 95.4%-calibrated age range between 671 and 876; Ref. Lyon-16233 (RICH), Fig. 9b). However, the charcoal was not found at the bottom of the kiln, thus raising the question of the significance of the age obtained. As a result, neither the archeointensity (due to the nature of the intensity variations during the High Middle Ages) nor the radiocarbon data (and their combination) make it possible to constrain the age of the beginning of ceramic production (Fig. 9). In particular, it seems useful to ask whether the stylistic features that led to the early dating of the 10<sup>th</sup> century could in fact have appeared somewhat earlier (last decades of the 9<sup>th</sup> c. or first decade of 10<sup>th</sup> c.) in the Vexin Français area than in other parts of the Ile-de-France region. This issue is still unresolved. Clearly, only additional archeological constraints, from the excavation of other kilns in the Vexin Français or the recognition of this ceramic production in occupation contexts, would further limit the age span of the production.

## 8. Conclusions

Seven new archeointensity values with accurate dating in the High Middle Ages further improved our knowledge of the variations in geomagnetic intensities in France, and more generally in Western Europe, over the past 1700 years.

Two regional modeling approaches were used to trace these variations, the first derived from the method of Thébault and Gallet (2010), which now considers irregularly spaced knots according to the data distribution, the second developed by Livermore et al. (2018) based on a transdimensional Bayesian technique. In addition, two databases were used that differ according to a criterion of data homogeneity, all of which are located within a 700 km circle around the city of Beaune. This dual approach allowed us to illustrate the sensitivity of the mean curves, based on the distribution of a large set of individual models, to the principles of each of the two modeling approaches. While the first method gives a very regular and smooth evolution in intensity variation, with a weighting of the effects linked to slightly discordant data, the second approach shows more abrupt variations with sometimes stronger amplitudes.

We also illustrated two examples of dating integrating the constraints resulting from the archeointensity results, in addition to those of the available archeological and radiocarbon data. For this, we also used two different dating techniques, either by classically comparing the intensity value to be dated with the reference geomagnetic variation curve, or by analyzing the marginal posterior age distribution of the data point given by the method of Livermore et al (2018). We showed that for France, the two techniques give very similar results. In this respect, the consideration of two different approaches for both regional field modeling and dating strengthens the interpretation of archeointensities for archeological dating.



Finally, beyond the information provided to the archeologists, our study showed that it would certainly be illusory to consider archeointensities as a fully independent “absolute” dating method (e.g. Aitken, 1990; Korte et al., 2019), especially in the absence of direction-based archeomagnetic constraints. On the contrary, archeointensities may provide chronological constraints, which in combination with other archeological and/or radiocarbon dating elements, can be very valuable in refining the dating of the structures/artifacts studied, opening the way to a wide range of complementary research on Medieval pottery production.

## **Acknowledgment**

We are very grateful to Maxime Le Goff for his constant support in the Triaxe measurements and for fruitful discussions around the intensity results. We also thank Caroline Claude from INRAP who was helpful in the selection of medieval groups of pottery fragments. We further thank the two anonymous reviewers and the guest editor Annick Chauvin for their useful comments. This is IPGP contribution no. 4220.

## **References**

- Aidona, E., Polymeris, G., Camps, P., Kondopoulou, D., Ioannidis, N., Raptis, K., 2018. Archaeomagnetic versus luminescence methods: the case of an Early Byzantine ceramic workshop in Thessaloniki, Greece. *Archaeological and Anthropological Sciences* 10. <https://doi.org/10.1007/s12520-017-0494-5>
- Aitken, M., 1990. *Science-Based Dating in Archaeology*. Taylor & Francis Ltd, 294 pp.
- Batt, C.M., Brown, M.C., Clelland, S.-J., Korte, M., Linford, P., Outram, Z., 2017. Advances in archaeomagnetic dating in Britain: new data, new approaches and a new calibration curve. *J. Archaeol. Sci.* 85, 66–82, <https://doi.org/10.1016/j.jas.2017.07.002>

694 Biggin, A.J., Poidras, T., 2006. First-order symmetry of weak-field partial thermoremanence  
 695 in multi-domain ferromagnetic grains. 1. Experimental evidence and physical  
 696 implications. *Earth Planet Sci. Lett.* 245, 438–453,  
 697 <https://doi.org/10.1016/j.epsl.2006.02.035>

698 Bouillon, J., (Dir.), 2015. Loiret, Saran, Ancienne route de Chartres, au lieu-dit « La  
 699 Guignace » - (zone sud et zone nord). Une extension nord au complexe artisanal potier de  
 700 Saran « La Médecinerie » (VIe-Xe siècle), Rapport de fouille, INRAP Centre Île-de-  
 701 France.

702 Brown, M. C, Hervé, G., Korte, M., Genevey A., Global archaeomagnetic data: the state of  
 703 the art and future challenges. *Phys. Earth Planet. Inter.*, accepted with minor revisions.

704 Bucur, I., 1994. The direction of the terrestrial magnetic field in France during the last 21  
 705 centuries. *Phys. Earth Planet. Inter.* 87, 95–109, [https://doi.org/10.1016/0031-](https://doi.org/10.1016/0031-9201(94)90024-8)  
 706 [9201\(94\)90024-8](https://doi.org/10.1016/0031-9201(94)90024-8)

707 Buffett, B., Knezek, N., Holme, R., 2016. Evidence for MAC waves at the top of Earth's core  
 708 and implications for variations in length of day, *Geophysical Journal International*, 204,  
 709 3, 1789–1800, <https://doi.org/10.1093/gji/ggv552>

710 Casas, L., Shaw, J., Gich, M., Share, J.A., 2005. High-quality microwave archaeointensity  
 711 determinations from an early 18th century AD English brick kiln. *Geophys. J. Int.* 161,  
 712 653–661, <https://doi.org/10.1111/j.1365-246X.2005.02631.x>

713 Casas, L., Tema, E., 2019. Investigating the expected archaeomagnetic dating precision in  
 714 Europe: A temporal and spatial analysis based on the SCHA.DIF.3K geomagnetic field

715 model, *Journal of Archaeological Science* 108, 104972,  
716 <https://doi.org/10.1016/j.jas.2019.104972>

717 Catanzariti, G., McIntosh, G., Osete, M., Nakamura, T., Rakowski, A., González, I., Lanos,  
718 P., 2007. A Comparison of Radiocarbon and Archaeomagnetic Dating from an  
719 Archaeological Site in Spain, *Radiocarbon* 49, 2, 543-550,  
720 <https://doi.org/10.1017/S0033822200042454>

721 Chaudriller, S., (Dir.), 2019. Hermé, « Les Malletons » (carrière S.P.M.), Rapport de fouille,  
722 INRAP Centre - Île-de-France - Seine-et-Marne.

723 Chauvin, A., Garcia, Y., Lanos, P., Laubenheimer, F., 2000. Paleointensity of the  
724 geomagnetic field recovered on archaeomagnetic sites from France. *Phys. Earth Planet.*  
725 *Int.* 120, 111–136, [https://doi.org/10.1016/S0031-9201\(00\)00148-5](https://doi.org/10.1016/S0031-9201(00)00148-5)

726 Coe, R. S., 1967. Paleo-intensities of the Earth's magnetic field determined from Tertiary and  
727 Quaternary rocks. *J. Geophys. Res.* 72, 3247–3262,  
728 <https://doi.org/10.1029/JZ072i012p03247>

729 Dekkers, M.J., Böhnell, H.N., 2006. Reliable absolute palaeointensities independent of  
730 magnetic domain state. *Earth Planet. Sci. Lett.* 248, 508–517.  
731 <https://doi.org/10.1016/j.epsl.2006.05.040>

732 Donadini, F., Kovacheva, M., Kostadinova, M., Hedley, I.G., Pesonen, L.J., 2008.  
733 Palaeointensity determination on an early medieval kiln from Switzerland and the effect  
734 of cooling rate. *Phys. Earth. Planet. Int.* 33, 449–457,  
735 <https://doi.org/10.1016/j.pce.2008.02.019>

736 Donadini, F., Motschi, A., Rösch, C., Hajdas, I., 2012. Combining an archaeomagnetic and  
 737 radiocarbon study: dating of medieval replaces at the Mühlegasse. Zürich. *J. Archaeol.*  
 738 *Sci.* 39, 2153–2166, <https://doi.org/10.1016/j.jas.2012.02.030>

739 Ech-Chakrouni, S., Hus, J., Spassov, S., 2013. Constraints of archaeomagnetic dating and  
 740 field intensity determinations in three ancient tile kilns in Belgium. *Stud Geophys*  
 741 *Geod* 57, 585–604, <https://doi.org/10.1007/s11200-012-0779-1>

742 Fabian, K., Leonhardt, R., 2010. Multiple-specimen absolute paleointensity determination: an  
 743 optimal protocol including pTRM normalization, domain-state correction, and alteration  
 744 test. *Earth Planet. Sci. Lett.* 297, 84–94, <https://doi.org/10.1016/j.epsl.2010.06.006>

745 Gallet, Y., Genevey, A., Le Goff, M., 2002. Three millennia of directional variation of the  
 746 Earth's magnetic field in western Europe as revealed by archeological artifacts. *Phys.*  
 747 *Earth. Planet. Inter.* 131, 81–89, [https://doi.org/10.1016/S0031-9201\(02\)00030-4](https://doi.org/10.1016/S0031-9201(02)00030-4)

748 Gallet, Y., Le Goff, M., 2006. High-temperature archeointensity measurements from  
 749 Mesopotamia. *Earth and Planetary Science Letters.* 241, 159-173.,  
 750 <https://doi.org/10.1016/j.epsl.2005.09.058>

751 Gallet, Y., Genevey, A., Le Goff, M., Warmé, N., Gran-Aymerich, J., Lefèvre, A., 2009. On  
 752 the use of archeology in geomagnetism, and vice-versa: Recent developments in  
 753 archeomagnetism, *C. R. Physique* 10, 630–648, [https://doi.org](https://doi.org/10.1016/j.crhy.2009.08.005)  
 754 [/10.1016/j.crhy.2009.08.005](https://doi.org/10.1016/j.crhy.2009.08.005)

755 Gallet, Y., Genevey, A., Margueron, J.-C., Le Goff, M., Thébault, E., Matthiae, P., Butterlin,  
 756 P., Al Maqdissi, M., 2014a. Exemples de chronologie archéomagnétique à Mari/Tell  
 757 Hariri, Syria, Mari, ni Est, ni Ouest, suppl. 2, 217-230

758 Gallet, Y., D'Andrea, M., Genevey, A., Pinnock, F., Le Goff, M., Matthiae, P., 2014b.  
759 Archaeomagnetism at Ebla (Tell Mardikh, Syria). New data on geomagnetic field  
760 intensity variations in the Near East during the Bronze Age. *Journal of Archaeological*  
761 *Science*. 42. 295–304, <https://doi.org/10.1016/j.jas.2013.11.007>

762 Gallet, Y., Fortin, M., Fournier, A., Le Goff, M., & Livermore, P., 2020. Analysis of  
763 geomagnetic field intensity variations in Mesopotamia during the third millennium BC  
764 with archeological implications. *Earth and Planetary Science Letters* 537, 1–13,  
765 <https://doi.org/10.1016/j.epsl.2020.116183>

766 Genevey, A., Gallet, Y., 2002. Intensity of the geomagnetic field in western Europe over the  
767 past 2000 years: new data from ancient French pottery. *J. Geophys. Res.* 107 (B11),  
768 2285, <https://doi.org/10.1029/2001JB000701>

769 Genevey, A., Gallet, Y., Margueron, J., 2003. Eight thousand years of geomagnetic field  
770 intensity variations in the eastern Mediterranean. *J. Geophys. Res. B Solid Earth* 108 (5).  
771 EPM1-1-1-18. <https://doi.org/10.1029/2001JB001612>

772 Genevey, A., Gallet, Y., Constable, C.G., Korte, M., Hulot, G., 2008. ArcheoInt: an up-  
773 graded compilation of geomagnetic field intensity data for the past ten millennia and its  
774 application to the recovery of the past dipole moment. *Geochem. Geophys. Geosyst.* 9,  
775 Q04038, <https://doi.org/10.1029/2007GC001881>

776 Genevey, A., Gallet, Y., Rosen, J., Le Goff, M., 2009. Evidence for rapid geomagnetic field  
777 intensity variations in Western Europe over the past 800 years from new archeointensity  
778 French data. *Earth Planet. Sci. Lett.* 284, 132–143,  
779 <https://doi.org/10.1016/j.epsl.2009.04.024>

780 Genevey, A., Gallet, Y., Thébault, E., Jesset, S., Le Goff, M., 2013. Geomagnetic field  
 781 intensity variations in Western Europe over the past 1100 years. *Geochem. Geophys.*  
 782 *Geosyst.* 14/8, 2858–2872, <https://doi.org/10.1002/ggge.20165>

783 Genevey, A., Gallet, Y., Jesset, S., Thébault, E., Bouillon, J., Lefèvre, A., Le Goff, M., 2016.  
 784 New archeointensity data from French early medieval ceramic production (6th-10th  
 785 century AD). Tracing 1500 years of geomagnetic field intensity variations in Western  
 786 Europe. *Phys. Earth Planet Inter.* 257, 205–219,  
 787 <https://doi.org/10.1016/j.pepi.2016.06.001>

788 Genevey, A., Principe, C., Gallet, Y., Clemente, G., Le Goff, M., Fournier, A., Pallecchi, P.,  
 789 2019. Refining the high-fidelity archaeointensity curve for western Europe over the past  
 790 millennium: analysis of Tuscan architectural bricks (Italy). *Geological Society of*  
 791 *London.* SP497, <https://doi.org/10.6084/m9.figshare.c.4728257>

792 Gómez-Paccard, M., Beamud, E., 2008. Recent achievements in archaeomagnetic dating in  
 793 the Iberian Peninsula: application to Roman and Mediaeval Spanish structures, *Journal of*  
 794 *Archaeological Science* 35, 1389-1398, <https://doi.org/10.1016/j.jas.2007.10.005>

795 Gómez-Paccard, M., Chauvin, A., Lanos, P., Dufresne, P., Kovacheva, M., Hill, M.J.,  
 796 Beamud, E., Blain, S., Bouvier, A., Guibert, P. Archaeological Working Team, 2012.  
 797 Improving our knowledge of rapid geomagnetic field intensity changes observed in  
 798 Europe between 200 and 1400 AD. *Earth Planet. Sci. Lett.* 355– 356, 131–143,  
 799 <https://doi.org/10.1016/j.epsl.2012.08.037>

800 Hartmann, G.A., Genevey, A., Gallet, Y., Trindade, R.I.F., Etchevarne, C., Le Goff, M.,  
 801 Afonso, M.C., 2010. Archeointensity in Northeast Brazil over the past five centuries.  
 802 *Earth Planet. Sci. Lett.* 296, 340–352, <https://doi.org/10.1016/j.epsl.2010.05.016>

803 Hartmann, G.A., Genevey, A., Gallet, Y., Trindade, R.I.F., Le Goff, M., Najjar, R.,  
 804 Etchevarne, C., Afonso, M.C., 2011. New historical archeointensity data from Brazil:  
 805 Evidence for a large regional non-dipole field contribution over the past few centuries.  
 806 Earth Planet. Sci. Lett. 306, 66–76. <https://doi.org/10.1016/j.epsl.2011.03.030>

807 Hellio, G., Gillet, N., Bouligand, C., Jault, D., 2014. Stochastic modelling of regional  
 808 archaeomagnetic series. Geophys. J. Int. 199 (2), 931–943,  
 809 <https://doi.org/10.1093/gji/ggu303>

810 Herries, A., Kovacheva, M., Kostadinova-Avramova, M., 2008. Mineral magnetism and  
 811 archaeomagnetic dating of a mediaeval oven from Zlatna Livada, Bulgaria. Physics and  
 812 Chemistry of The Earth 33. <https://doi.org/10.1016/j.pce.2008.02.021>

813 Hervé, G., Lanos, P., 2017. Improvements in Archaeomagnetic Dating in Western Europe  
 814 from the Late Bronze to the Late Iron Ages: An Alternative to the Problem of the  
 815 Hallstattian Radiocarbon Plateau: Improvements in archaeomagnetic dating in Western  
 816 Europe. Archaeometry. <https://doi.org/10.1111/arc.12344>

817 Hervé, G., Faßbinder, J., Gilder, S. A., Metzner-Nebelsick, C., Gallet, Y., Genevey, A.,  
 818 Schnepf, E., Geisweid, L., Pütz, A., Reuß, S., Wittenborn, F., Flontas, A., Linke, R.,  
 819 Riedel, G., Walter, F., Westhausen, I., 2017. Fast geomagnetic field intensity variations  
 820 between 1400 and 400 BCE: New archeointensity data from Germany. Phys. Earth  
 821 Planet. Inter. 270, 143–156. <https://doi.org/10.1016/j.pepi.2017.07.002>

822 Hervé, G., Chauvin, A., Lanos, P., Rochette, P., Perrin, M., Perron d’Arc, M., 2019. Cooling  
 823 rate effect on thermoremanent magnetization in archaeological baked clays: an  
 824 experimental study on modern bricks. Geophys. J. Int. 217 (2), 1413–1424,  
 825 <https://doi.org/10.1093/gji/ggz076>

826     Jeset, S., (dir.), Saran (Loiret), « La Voie Nouvelle », Rapport de fouille, Ville d'Orléans, to  
827     be published.

828     Jones, S. A., Tauxe, L., Blinman, E., Genevey, A., 2020. Archeointensity of the Four Corners  
829     Region of the American Southwest. *Geochem. Geophys. Geosyst.* 21 (3),  
830     e2018GC007509, <https://doi.org/10.1029/2018GC007509>

831     Korte, M., Brown, M., Gunnarson, S., Nilsson, A., Panovska, S., & Wardinski, I., Constable,  
832     C., 2019. Refining Holocene geochronologies using palaeomagnetic records. *Quaternary*  
833     *Geochronology* 50. <https://doi.org/10.1016/j.quageo.2018.11.004>.

834     Kostadinova-Avramova, M., Jordanova, N., 2019. Study of cooling rate effect on baked clay  
835     materials and its importance for archaeointensity determinations. *Phys. Earth Planet.*  
836     *Inter.* 288, 9– 25, <https://doi.org/10.1016/j.pepi.2019.02.009>

837     Lanos, P., 2004. Bayesian Inference of Calibration Curves: Application to  
838     Archaeomagnetism. Springer London, London, 43–82.

839     Lanos, P., 2019. Physique de l'archéomagnétisme pour la datation de bâtiments du haut  
840     Moyen Âge, *Reflets phys.* 63, *Physique et matériaux anciens*.  
841     <https://doi.org/10.1051/refdp/201963054>

842     Lefèvre, A., Mahé, N., 2004. La céramique du haut Moyen Âge en Île-de-France à travers la  
843     fouille des habitats ruraux, *Revue Archéologique de Picardie*, n°3-4, 105-150.

844     Lefèvre, A., Peixoto, X., 2015. Les ateliers de potiers de la rue Gaudray à Vanves (Hauts-de-  
845     Seine). In: Thuillier, F., Louis, E. (Eds.), *Tourner autour du pot...*, Les ateliers de potiers  
846     médiévaux du Ve au XIIe siècle dans l'espace européen. publications du CRAHAM,  
847     Caen.



848 Livermore, P. W., Fournier, A., Gallet, Y., Bodin, T., 2018. Transdimensional inference of  
849 archeomagnetic intensity change. *Geophys. J. Int.* 215 (3), 2008–2034,  
850 <https://doi.org/10.1093/gji/ggy383>

851 Livermore, P.W., Gallet, Y., Fournier, A., 2021. Archaeomagnetic intensity variations during  
852 the era of geomagnetic spikes in the Levant, *Phys. Earth Planet. Inter.* 312,  
853 <https://doi.org/10.1016/j.pepi.2021.106657>

854 Le Goff, M., Gallet, Y., Genevey, A., Warmé, N., 2002. On archaeomagnetic secular  
855 variation curves and archaeomagnetic dating. *Phys. Earth Planet. Inter.* 134, 203–211,  
856 [https://doi.org/10.1016/S0031-9201\(02\)00161-9](https://doi.org/10.1016/S0031-9201(02)00161-9)

857 Le Goff, M., Gallet, Y., 2004. A new three-axis vibrating sample magnetometer for  
858 continuous high-temperature magnetization measurements: applications to paleo- and  
859 archeo-intensity determinations. *Earth Planet. Sci. Lett.* 229, 31–43,  
860 <https://doi.org/10.1016/j.epsl.2004.10.025>

861 Le Goff, M., Gallet, Y., Warmé, N., Genevey, A., 2020. An updated archeomagnetic  
862 directional variation curve for France over the past two millennia, following 25 years of  
863 additional data acquisition, *Physics of the Earth and Planetary Interiors*, 309,  
864 <https://doi.org/10.1016/j.pepi.2020.106592>

865 López-Sánchez, J., McIntosh, G., Osete, M. L., Del Campo, A., Villalaín, J. J., Pérez, L.,  
866 Kovacheva, M., Rodríguez de la Fuente, O., 2017. Epsilon iron oxide: Origin of the high  
867 coercivity stable low Curie temperature magnetic phase found in heated archeological  
868 materials. *Geochemistry, Geophysics, Geosystems.* 18.  
869 <https://doi.org/10.1002/2017GC006929>

870 López-Sánchez, J., Palencia-Ortas, A., Del Campo, A., McIntosh, G., Kovacheva, M., Martín-  
 871 Hernández, F., Carmona, N., Rodríguez de la Fuente, O., Marín, P., Molina-Cardín, A.,  
 872 Osete, M.L., 2020 Further progress in the study of epsilon iron oxide in archaeological  
 873 baked clays, *Phys. Earth Planet. Inter.* 307. <https://doi.org/10.1016/j.pepi.2020.106554>

874 Lowrie, W., 1990. Identification of ferromagnetic minerals in a rock by coercivity and  
 875 unblocking temperatures properties. *Geophys. Res. Lett.* 17, 159–162.  
 876 <http://dx.doi.org/10.1029/GL017i002p00159>.

877 Mahé, N., (Dir.), 2020. Chamigny, Rue de la Marne - RD 80 - Lieu-dit « La Grande  
 878 Maison », Rapport de fouille, INRAP Île-de-France, Seine-et-Marne.

879 Marot, E., (Dir.), 2017. La Chapelle Saint-Ursin, l'Angoulaire, chemin des vallées aux  
 880 Fruscades, Trajectoires antique et alto-médiévale d'un établissement agricole de la  
 881 proche campagne de Bourges-Avaricum, Rapport final d'opération de fouilles  
 882 archéologiques, Région Centre - Val de Loire - Département du Cher (18), Bourges Plus.

883 Pavón-Carrasco, F.J., Osete, M.L., Torta, J.M., Gaya-Pique, L.R., 2009. A regional  
 884 archeomagnetic model for Europe for the last 3000 years, *SCHA.DIF.3K: Applications to*  
 885 *archeomagnetic dating. Geochem. Geophys. Geosyst.* 10, Q03013.  
 886 <https://doi.org/10.1029/2008GC002244>

887 Pavón-Carrasco, F.J., Rodríguez-González, J., Osete, M. L., Torta, J. M., 2011. A MATLAB  
 888 tool for archaeomagnetic dating. *Journal of Archaeological Science* 38, 408-419,  
 889 <https://doi.org/10.1016/j.jas.2010.09.021>

890 Pavón-Carrasco, F. J., Campuzano, S. A., Rivero-Montero, M., Molina-Cardín, A., Gómez-  
 891 Paccard, M., & Osete, M.L., 2021. *SCHA.DIF.4k: 4,000 years of paleomagnetic*

892 reconstruction for Europe and its application for dating. *Journal of Geophysical Research:*  
893 *Solid Earth*, 126, e2020JB021237. <https://doi.org/10.1029/2020JB021237>

894 Principe, C., Gogichaishvili, A., Arrighi, S., Devidze, M., La Felice, S., Paolillo, A.,  
895 Giordano, D., Morales, J., 2018. Archaeomagnetic dating of Copper Age furnaces at  
896 Croce di Papa village and relations on Vesuvius and Phlegraean Fields volcanic activity,  
897 *Journal of Volcanology and Geothermal Research* 349, 217-229,  
898 <https://doi.org/10.1016/j.jvolgeores.2017.11.002>

899 Regnard, S., 1999. Vienne-en-Arthies (Val-d'Oise). Hameau de Chaudry-La Pierre Percée,  
900 *Archéologie médiévale* 29, 372.

901 Regnard, S., Fayet, F., Genevey, A., Kucab, A., Regnard, A., Mousterde, P., Verasdonck, P.  
902 2021. Un atelier de potier du IX<sup>e</sup> siècle au hameau de Chaudry à Vienne-en-Arthies (Val-  
903 d'Oise), *Revue archéologique du Vexin français et du Val-d'Oise*, 45, 101-157.

904 Reimer, P., Austin, W., Bard, E., Bayliss, A., Blackwell, P., Ramsey, C., Butzin, M., Cheng,  
905 H., Edwards, R., Friedrich, M., Grootes, P., Guilderson, T., Hajdas, I., Heaton, T., Hogg,  
906 A., Hughen, K., Kromer, B., Manning, S., Muscheler, R., Palmer, J., Pearson, C., van der  
907 Plicht, J., Reimer, R., Richards, D., Scott, E., Southon, J., Turney, C., Wacker, L.,  
908 Adolphi, F., Büntgen, U., Capano, M., Fahrni, S., Fogtmann-Schulz, A., Friedrich, R.,  
909 Köhler, P., Kudsk, S., Miyake, F., Olsen, J., Reinig, F., Sakamoto, M., Sookdeo, A.,  
910 Talamo, S., 2020. The IntCal20 Northern Hemisphere radiocarbon age calibration curve  
911 (0-55 Cal kBP). *Radiocarbon* 62, 725–757.

912 Schnepf, E., Obenaus, M., Lanos, P., 2015. Posterior archaeomagnetic dating: An example  
913 from the Early Medieval site Thunau am Kamp, Austria. *Journal of Archaeological*  
914 *Science: Reports* 2, 688-698. <https://doi.org/10.1016/j.jasrep.2014.12.002>

915 Schnepf, E., Thallner, D., Arneitz, P., Leonhardt, R., 2020. New archeomagnetic secular  
 916 variation data from Central Europe, II: Intensities, *Phys. Earth Planet. Inter.* 309,  
 917 <https://doi.org/10.1016/j.pepi.2020.106605>

918 Shaar, R., Bechar, S., Finkelstein, I., Gallet, Y., Martin, M. A. S., Ebert, Y., Keinan, J.,  
 919 Gonen, L., 2020. Synchronizing geomagnetic field intensity records in the Levant  
 920 between the 23rd and 15th Centuries BCE: Chronological and methodological  
 921 implications. *Geochem. Geophys. Geosyst.* 21, 12,  
 922 <https://doi.org/10.1029/2020GC009251>

923 Shaw, J., 1974. A new method of determining the magnitude of the palaeomagnetic field:  
 924 Application to five historic lavas and five archaeological samples. *Geophys. J. R. Astron.*  
 925 *Soc.* 39, 133–141. <https://doi.org/10.1111/j.1365-246X.1974.tb05443.x>

926 Tema, E., Fantino, F., Ferrara, E., Allegretti, S., Giudice, A., Re, A., Barelo, F., Vella, S.,  
 927 Cirillo, L., Gulmini, M., 2014. Archaeological, archaeomagnetic and  
 928 thermoluminescence investigation of a baked clay kiln excavated at Chieri, northern  
 929 Italy: contribution to the rescue of our cultural heritage. *Annals of Geophysics* 57,  
 930 G0548, <https://doi.org/10.4401/ag-6611>

931 Thébault, E., Gallet, Y., 2010. A bootstrap algorithm for deriving the archeomagnetic field  
 932 intensity variation curve in the Middle East over the past 4 millennia BC. *Geophys. Res.*  
 933 *Lett.* 37, L22303, <https://doi.org/10.1029/2010GL044788>

934 Thellier, E., Thellier, O., 1959. Sur l'intensité du champ magnétique terrestre dans le passé  
 935 historique et géologique. *Ann. Geophys.* 15, 285–376.

Thellier, E., 1981. Sur la direction du champ magnétique terrestre en France durant les deux derniers millénaires. *Phys. Earth Planet. Inter.* 24, 89–132, [https://doi.org/10.1016/0031-9201\(81\)90136-9](https://doi.org/10.1016/0031-9201(81)90136-9)

Troyano, M., Gallet, Y., Genevey, A., Pavlov, V., Fournier, A., Lagroix, F., Niyazova, M., Mirzaakhmedov, D., 2021. Analyzing the geomagnetic axial dipole field moment over the historical period from new archeointensity results at Bukhara (Uzbekistan, Central Asia). *Phys. Earth Planet. Inter.* 310, <https://doi.org/10.1016/j.pepi.2020.106633>.

#### **Figure captions:**

Figure 1: (a) Location of the archeological sites discussed in this paper. The pink circles indicate the sites associated with the seven new precisely-dated archeointensity results. The two pink circles bordered with purple indicate the sites where groups were collected for dating (the yellow area represents the so-called “Vexin Français” region). The blue circles indicate the geographical distribution of our intensity dataset (Genevey et Gallet, 2002; Gallet et al. 2009; Genevey et al., 2009, 2013, 2016, 2019). The green squares correspond to the sites of the selected data obtained by Chauvin et al. (2000), Donadini et al. (2008), Gómez Paccard et al. (2012) and Schnepf et al. (2020 in this volume). The circle with a radius of 700km is centered on the city of Beaune (Burgundy) to where the different intensity results were reduced. (b) Kiln 3060 unearthed at Hermé. Sampling for direction and intensity was concentrated on the central tongue of the Kiln (Group HERME04) ©N. Warmé, Inrap (c) Close-up of the pottery fragments found in kiln 2629 unearthed in Chamigny (Group CHAM03) ©C. Seng, Inrap.

Figure 2: Archeointensity results obtained for six groups (or pairs of groups) of fragments. Each curve corresponds to the analysis of a specimen and represents the intensity values (i.e. the  $R'(T_i)$  data) obtained over the temperature range  $T_{min}$ - $T_{max}$  where the primary TRM component was isolated (given in Supp Tab. 1). These examples show that for each specimen, the  $R'(T_i)$  data are nearly constant over the  $T_{min}$ - $T_{max}$  temperature interval, indicating that the magnetic mineralogy has maintained the same acquisition capability for both the NRM and the laboratory-TRM. Enhanced scatter observed at low temperatures, when the running temperature  $T_i$  is close to  $T_{min}$ , is due to the small NRM and laboratory-TRM fractions involved in the  $R'(T_i)$  ratios.

Figure 3: Examples of magnetic behavior for rejected fragments. (a, b) Two fragments for which a major alteration of the magnetic mineralogy was detected from low-field magnetic susceptibility versus temperature measurements. (c, d) Fragment for which the primary TRM component could not be reliably isolated in the thermal demagnetization diagram (c) and corresponding intensity diagram with non-constant intensity values (d). (e, f) Fragment with a single magnetization component observed between 100°C and 520°C in the thermal demagnetization diagram (e) but with decreasing intensity values over the same temperature range (f). In the demagnetization diagrams (c, e), the solid (resp. empty) circles represent the declinations (resp. inclinations) in specimen coordinates.

Figure 4: Thermal demagnetization of three-axis IRM components acquired in fields of 1.25, 0.4 and 0.2 T for six different fragments successfully analyzed in intensity and low-field magnetic susceptibility versus temperature curves (up to 500-520°C) for the same fragments.

Figure 5: Archeointensity data available within a 700 km radius around Beaune combining our dataset and other selected results (see details in the figure). The results of Donadini et al (2008) and Gómez Paccard et al. (2012) were modified as discussed in the text. Direct measurements are from <http://www.bcmf.fr/>. All data were reduced to the latitude of Beaune (47.03°N, 4.83°E)

Figure 6: Intensity variations curves in Western Europe over the past 1700 years. (a,b) Variation curves obtained using the Thébaud and Gallet (2010) method considering our dataset only (a) and our data combined with the other selected data (b). The curve in pink indicates the probability maxima and the pink dotted lines the 95% credible interval. (c,d) Variation curves obtained using the AH-RJMCMC method (Livermore et al., 2018) considering only our data (c) and together with the other selected data (d). The curves in red and blue show the probability maxima and the median values, respectively; the thin dotted lines in blue show the 95% credible interval. More details are given in the text and in supp Table 2. In all diagrams, the density distribution of individual models is shown according to a grey colour code scale (maximum probability of 0.15). Direct measurements are from <http://www.bcmf.fr/>. All data were reduced to the latitude of Beaune (47.03°N, 4.83°E).

Figure 7: Archeomagnetic dating obtained for the pottery workshop discovered at La Chapelle Saint Ursin site (BOUR# groups). (a) Archeointensity correlation dating: The variation curve is calculated using the AH-RJMCMC method developed by Livermore et al (2018) method and taking into account all the selected data (see text) available within 700 km radius of the city of Beaune (see Fig. 6d). The horizontal area in orange shows the intensity value ( $\pm 2\sigma$ ) to be dated. The dating is carried out by direct comparison with the calculated models ensemble. The age intervals (light blue area, right y-scale; see Table 2) are determined according to a

95.4% threshold value (horizontal blue line) which defines a highest density region. (b) Archeointensity marginalized dating (Livermore et al., 2018): The intensity value to be dated is incorporated with a large age interval (here between 400 and 1200) into the database used for the construction of the models using AH-RJMCMC. The diagram presents the marginal posterior age distribution derived for the data point concerned. As previously, different age intervals (light blue area; Table 2) are obtained according to a 95.4% threshold (horizontal blue line). The picture shows the kiln once excavated © E. Marot, Bourges plus.

Figure 8: Dating elements available for the pottery workshop discovered at La Chapelle Saint Ursin. (a) Archeointensity correlation dating. The variations curve displayed is calculated using the Thébault and Gallet (2010) method and all the data selected within the 700 km radius of the city of Beaune (see Fig. 6b). The Gaussian curve in red next to the intensity axis represents the intensity value to be dated. The age probability derived from the comparison of the BOUR overall mean value with the reference curve, taking into account their error bars, is represented both directly on the variation curve using a colour code and by a probability density curve reported along the age axis. The age interval shown between brackets is the most likely age range at a 95.4% threshold. The drawing represents a characteristic form of the production to be dated (©E. Marot, Bourges Plus). (b) This panel presents the archeological age interval, with a uniform probability density considered for the pottery production (black line), the probability density of the C14 data after calibration (in red) and the final age probability (in green) derived by combining the pdfs of the three dating elements (archeomagnetism of figure (a), archeological and C14).



Figure 9: Same legend as in Fig. 8 but the archeointensity value to be dated was obtained for the pottery workshop discovered at Chaudry. The drawing represents a characteristic form of this production ©S. Regnard, CRAVF.

## **Table captions**

Table 1: New archeointensity results obtained for the seven dated groups of fragments and for the two series of groups investigated for dating.

Table 2: Results of archeomagnetic dating obtained for the pottery workshops discovered at La Chapelle Saint Ursin (BOUR#) and Chaudry (CHAU#). Dating is carried out using two field modeling techniques, according to Thébaud and Gallet (2010) and Livermore et al. (2018), two databases and two different dating approaches, here referred to as “archeointensity correlation dating” and “archeointensity marginalized dating”. For Chaudry, the calculations are performed using the standard error of mean intensity value and by artificially increasing this error up to 1.5  $\mu$ T. See the text for more explanation. All age intervals are given with a 95.4% confidence level.

## **Supplementary information**

Supp. Figure 1: Cooling rate (CR) effect on the intensity data obtained by Donadini et al. (2008) and Gómez- Paccard et al. (2012). The results are reported at the site location, both at the specimen (spec.) and group levels. The description of the different symbols is given in the Figure. The “Nblue/Npink” numbers for the data obtained by Gómez- Paccard et al. (2012) indicate the number of results used to derive the mean value when using all the data, i.e. combining CR corrected and uncorrected values (Nblue), and the number of CR-corrected values used to derive the mean (Npink). The “Ngrey/Nyellow” number for the result of

Donadini et al. (2012) indicates the number of results obtained from small samples (volume 1 cm<sup>3</sup>) analyzed at the Helsinki paleomagnetic laboratory (Ngrey) and the number of large samples (volume 8 cm<sup>3</sup>) analyzed in the paleomagnetic laboratory at Sofia (Nyellow).

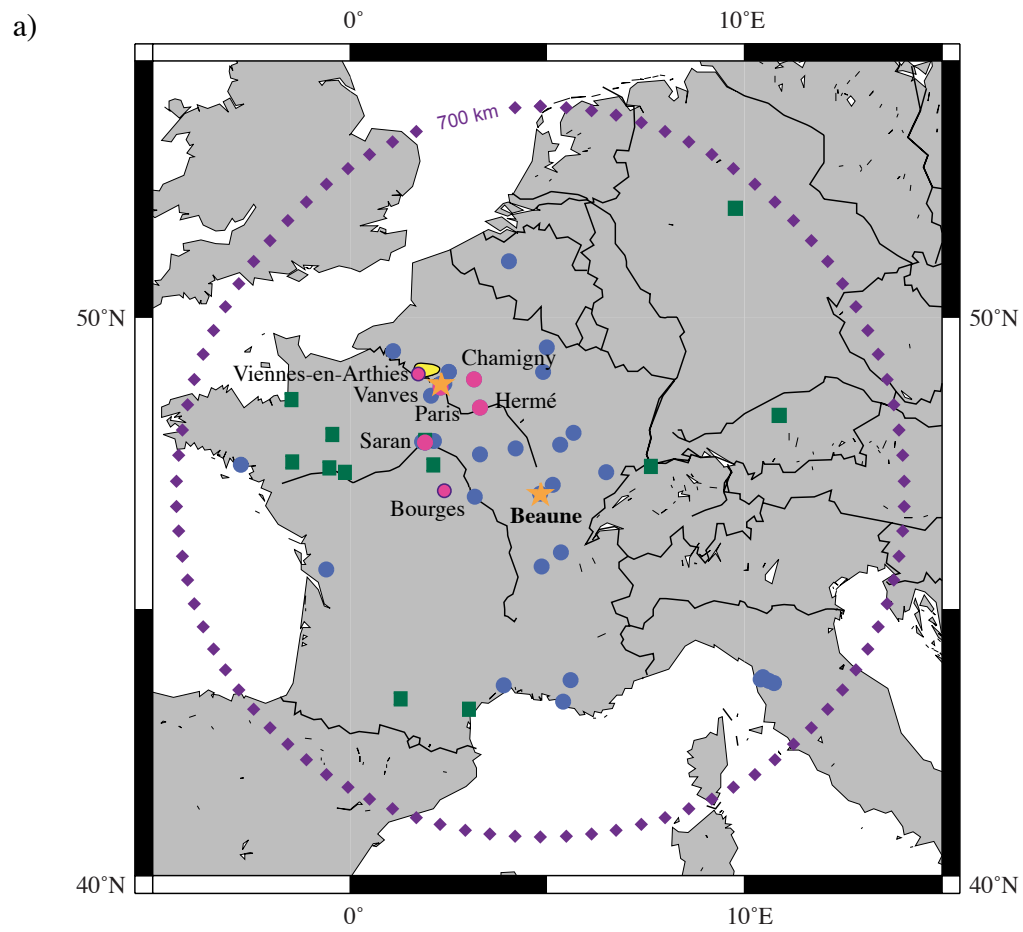
Supp. Figure 2: Archeomagnetic dating obtained for the pottery workshop discovered at the Chaudry site (CHAU# groups). (a) Archeointensity correlation dating: The variation curve is calculated using the AH-RJMCMC method developed by Livermore et al (2018) method and taking into account all the selected data (see text) available within the 700 km radius of the city of Beaune (see Fig. 6d). The horizontal area in orange shows the intensity value ( $\pm 2\sigma$ ) to be dated. The dating is carried out by direct comparison with the calculated models. The age intervals (light blue area, right y-scale; see Table 2) are determined according to a 95.4% threshold value (horizontal blue line). (b) Archeointensity marginalized dating (Livermore et al. 2018): The intensity value to be dated is incorporated with a large age interval (here between 400 and 1200) in the database used for the construction of the models. The diagram presents the marginal posterior age distribution derived for the data point concerned. As previously, different age intervals (light blue area; Table 2) are obtained according to a 95.4% threshold (horizontal blue line). The picture shows the kiln being excavated with its filling. © S. Regnard, CRAVF.

Supp. Table 1: Intensity results obtained at the specimen level and mean values obtained at the fragment level. ‘Natural magnetic moment’: Magnetic moment before demagnetization for each specimen in A.m<sup>2</sup>. The volume of each specimen is of the order of 0.75 cm<sup>3</sup> or slightly less. ‘Tmin-Tmax’: Interval of temperature involved for the intensity computation. ‘F lab’: Intensity of the laboratory field in  $\mu$ T. ‘NRM T1 (T1’)’: Fraction in % between the magnetization unblocked between Tmin and Tmax, thus used for intensity determination, and

the magnetization with unblocking temperatures  $\geq T_{min}$ . ‘Slope R’: Slope of the straight line computed by linear regression from the  $R'(T_i)$  data between  $T_{min}$  and  $T_{max}$ . It is calculated as follows (see also Gallet and Le Goff 2006):  $\text{Slope } R' = (R'(T_{max}) - R'(T_{min})) / (\text{Mean } R'(T_i) \text{ data})$  where  $R'(T_{max})$  and  $R'(T_{min})$  are here the values at  $T_{max}$  and  $T_{min}$  deriving from the linear regression of the  $R'(T_i)$  data. It is expressed in %. ‘F Triaxe’: Intensity values obtained at the specimen level in  $\mu T$ . It is estimated by computing the arithmetic mean from all  $R'(T_i)$  ratios obtained for a specimen over the  $T_{min}$ - $T_{max}$  temperature range. ‘F Triaxe mean value per fragment  $\pm \sigma F$ ’: Mean intensity value obtained at the fragment level with its standard error when computed from 2 values or its standard deviation when computed from 3 values.  $(N1/N2/N3/N4)^*$  indicates respectively the number of fragments collected, the number of fragments whose magnetization was strong enough relative to the Triaxe sensitivity, the number of fragments measured on the Triaxe for which no sign of magnetic mineralogy alteration was observed during the susceptibility measurements and the number of fragments retained to estimate a mean value at the group level.  $(n1/n2)^{**}$  indicates respectively the number of specimens measured using the Triaxe and the number of retained specimens. Note that we usually test two to three specimens per fragment to reject or retain the fragment based on our set of quality criteria.

Supp. Table 2: Intensity values derived from the method of Thébault and Gallet (2010; maximum probability and 95% credible interval) and that of Livermore et al (2018; maximum probability, median, 95% credible interval). For the latter technique, the following computational parameters were considered:  $\sigma_{move}=30$  years,  $\sigma_{change}=5 \mu T$ ,  $\sigma_{birth}=5 \mu T$ ,  $K_{max}=150$ , prior intensities between  $35 \mu T$  and  $95 \mu T$  and a chain length of 200 million samples. One datum age is perturbed per age-resampling. All the calculations are carried out

1105 using our data alone or our dataset combined with a selection of other results (see text). These  
1106 values trace the different curves shown in Fig. 6.



b)



c)



Figure 1.

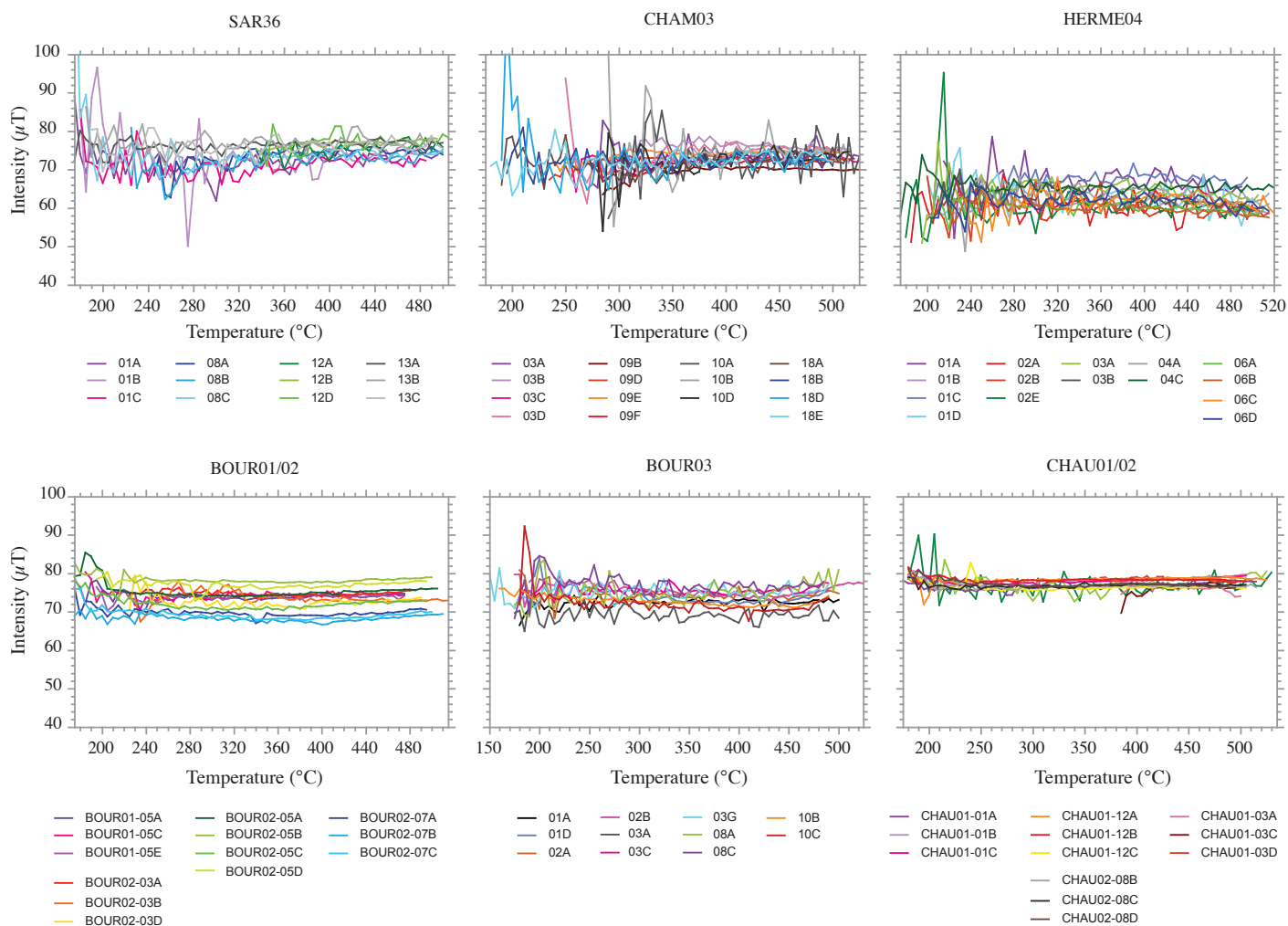


Figure 2.

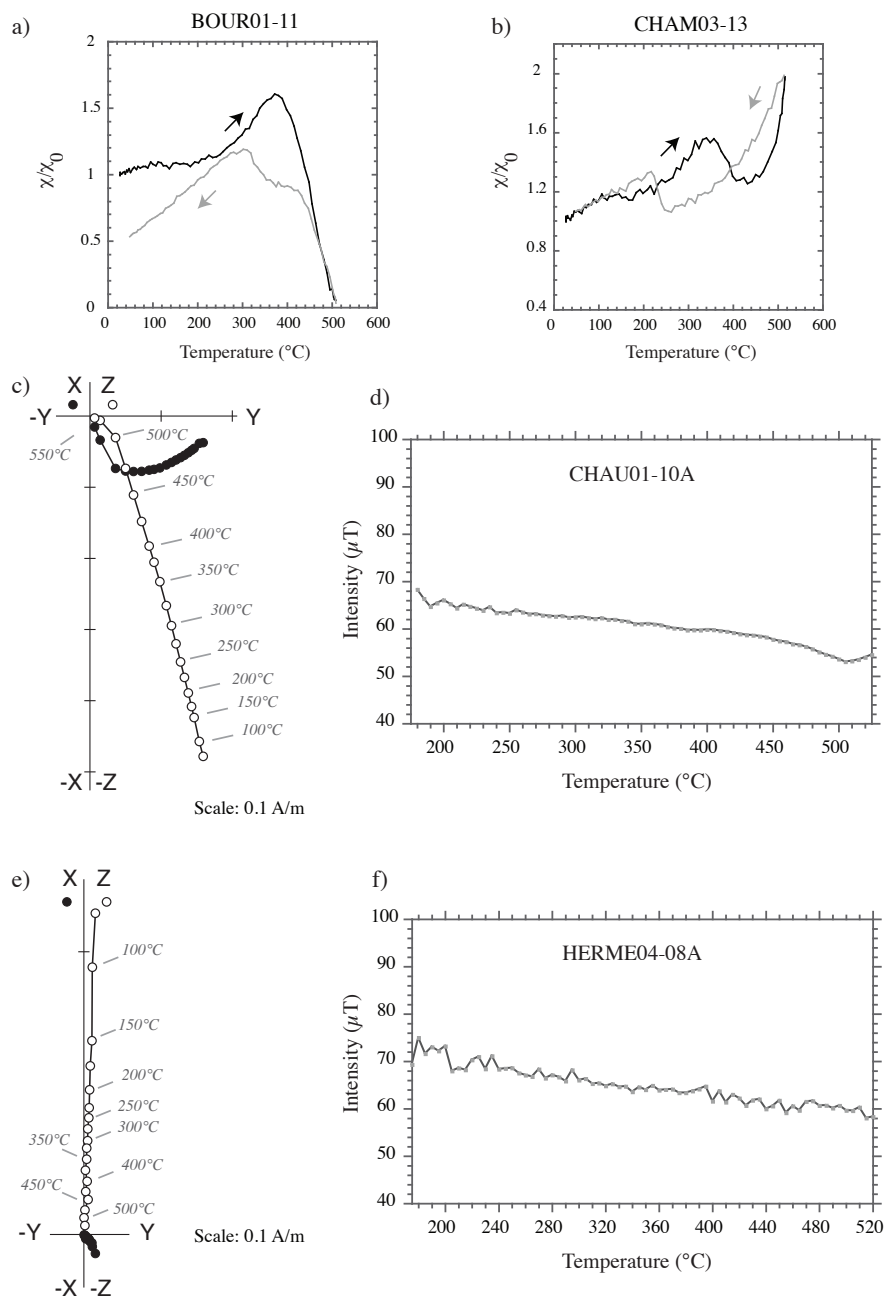


Figure 3.

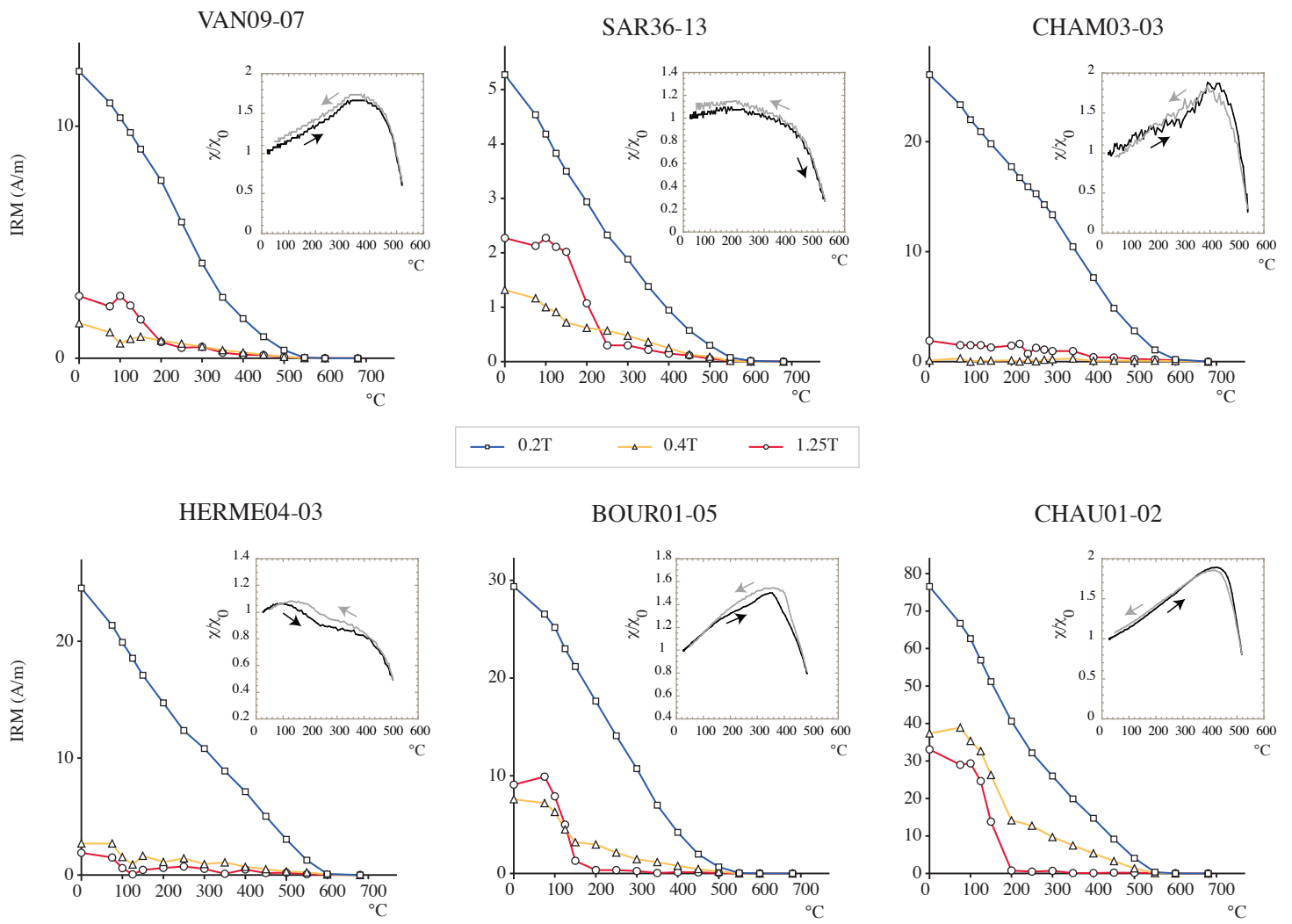


Figure 4.



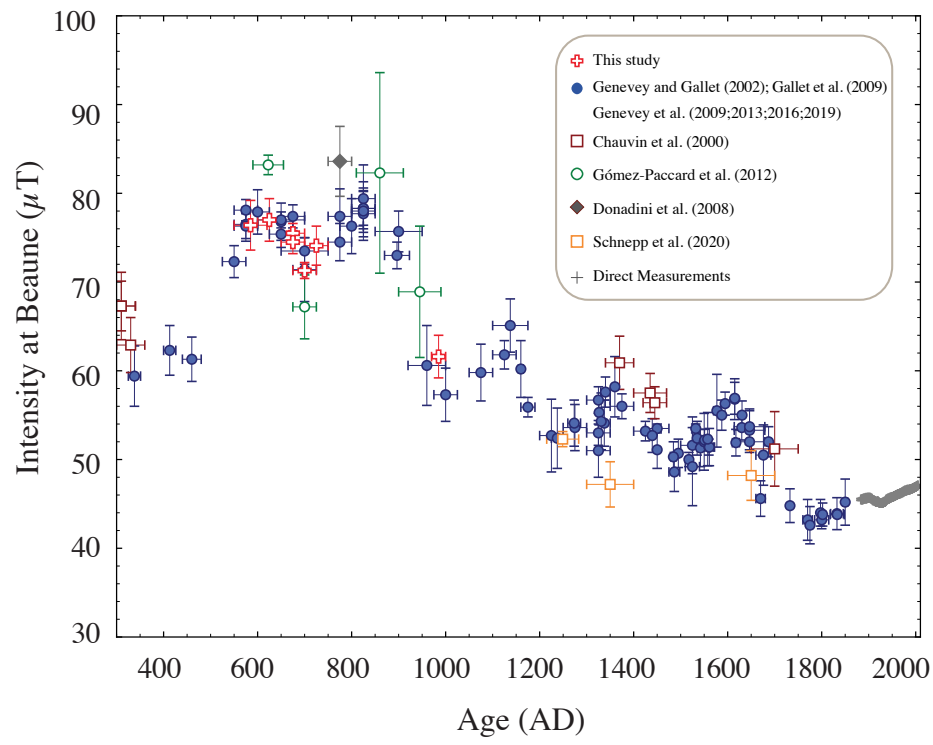


Figure 5.

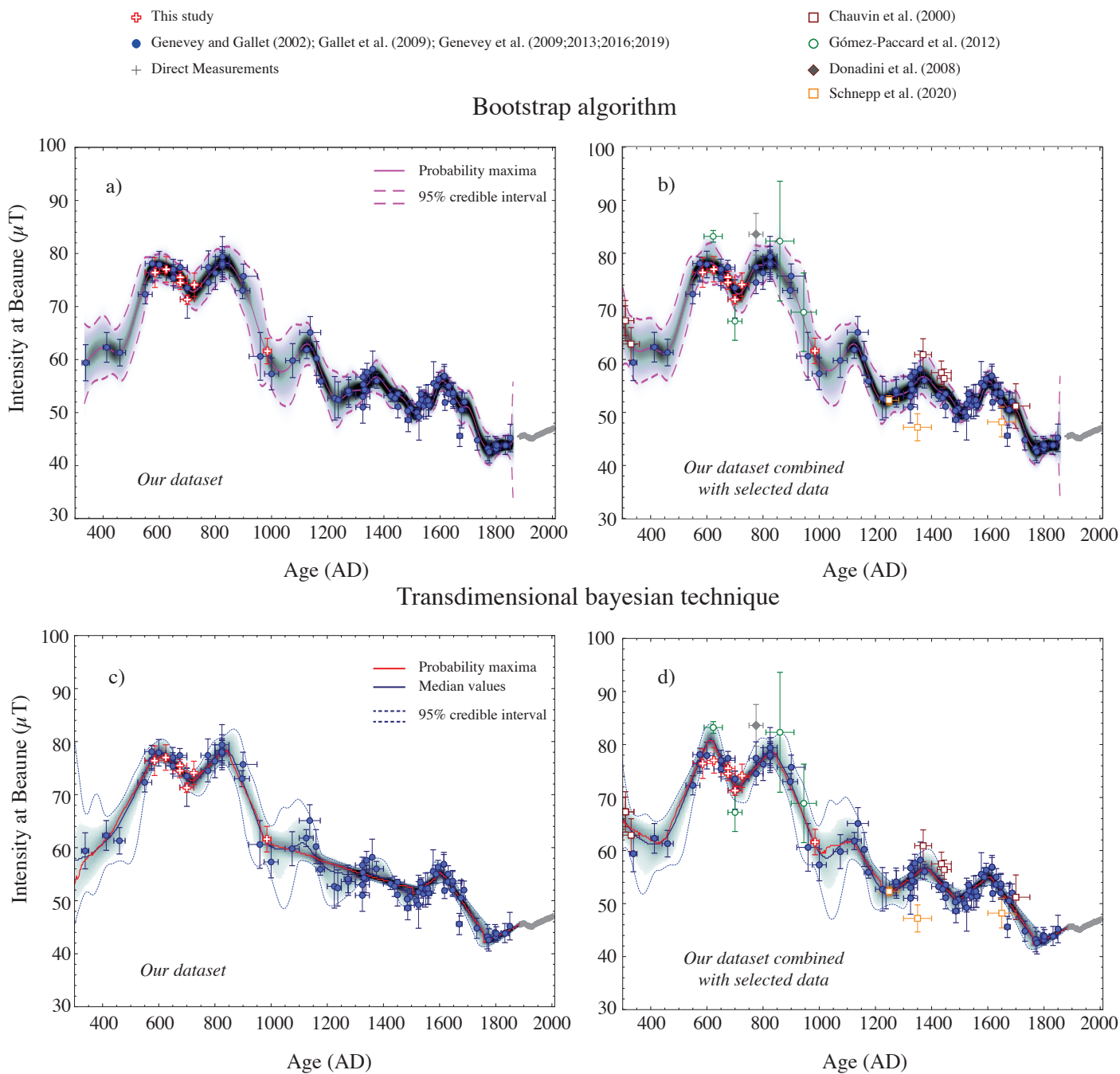


Figure 6.

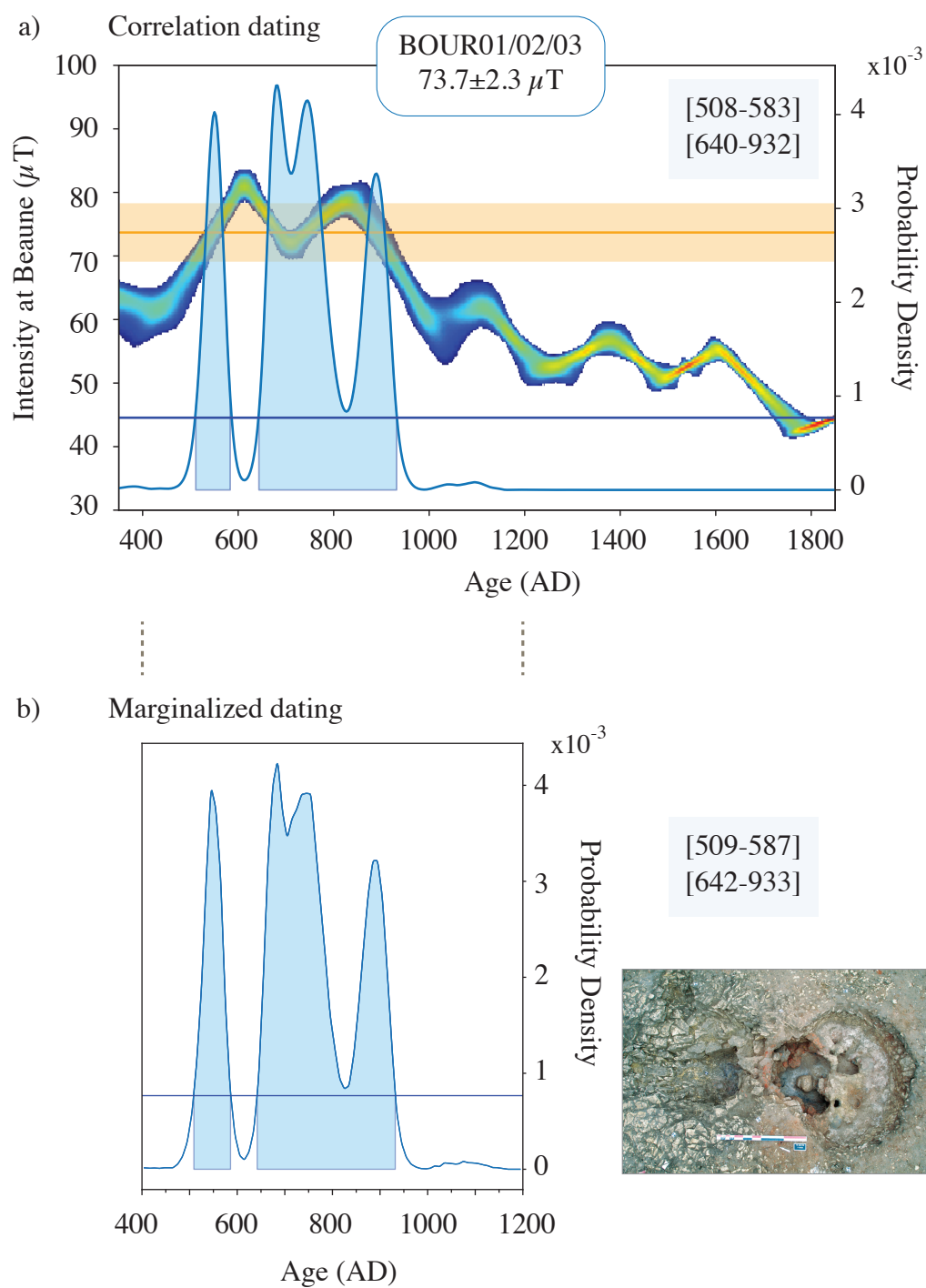


Figure 7

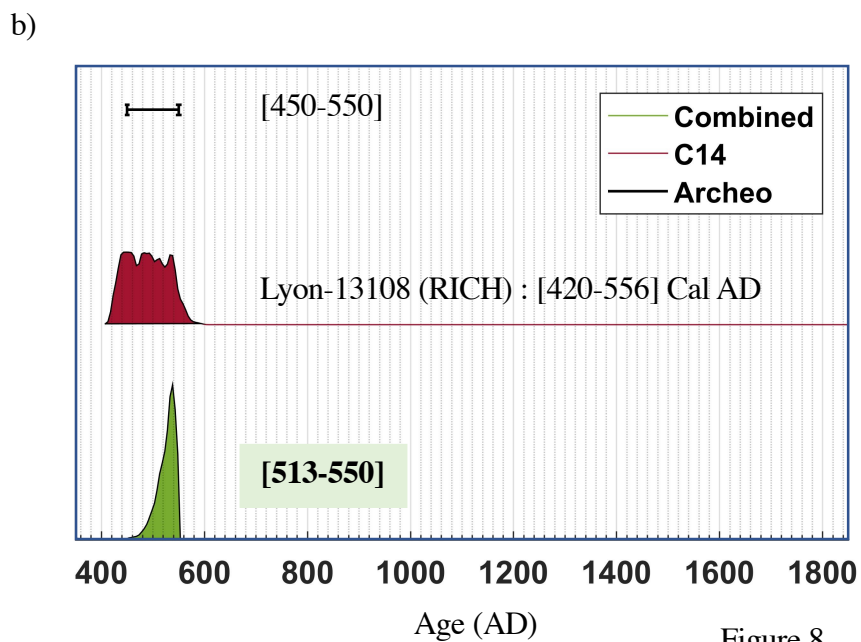
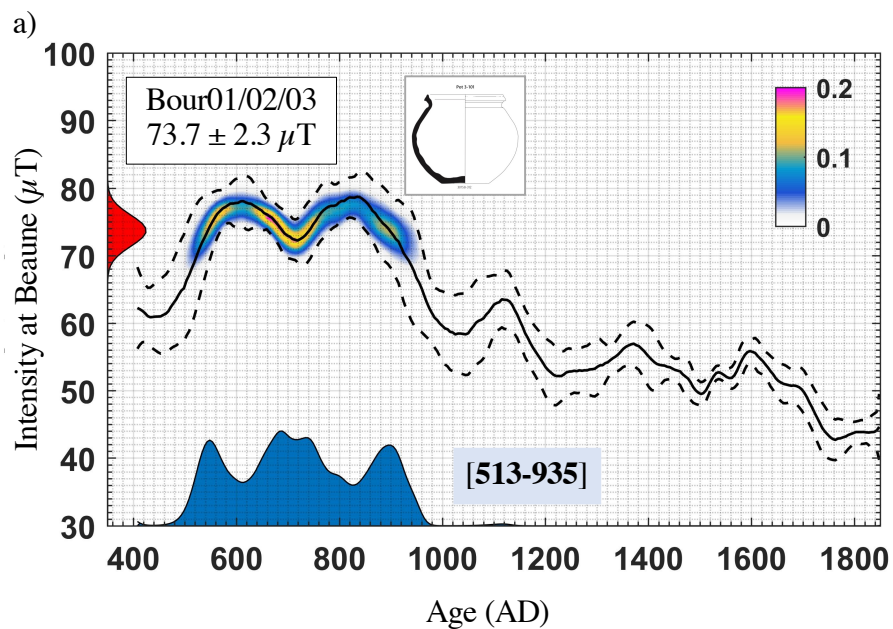


Figure 8.

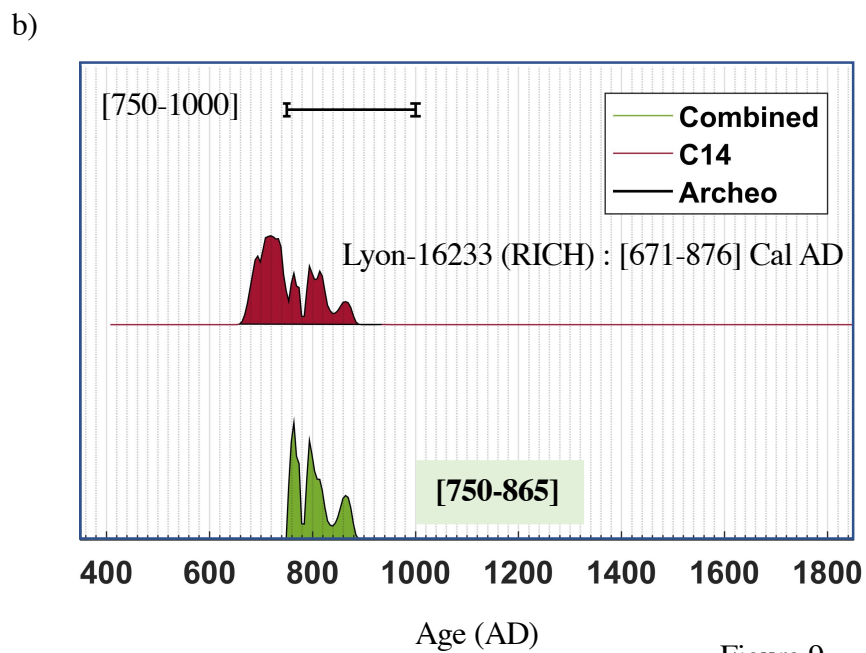
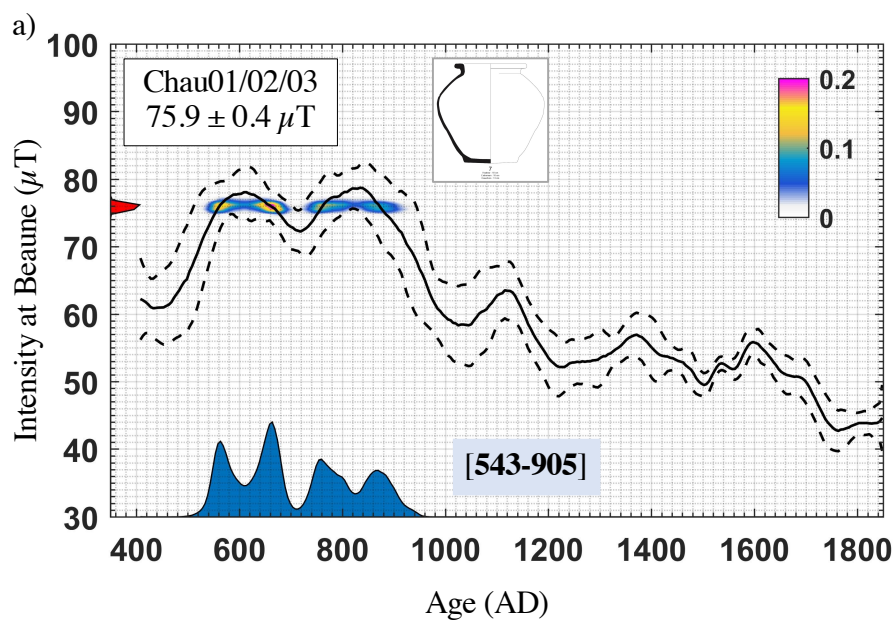


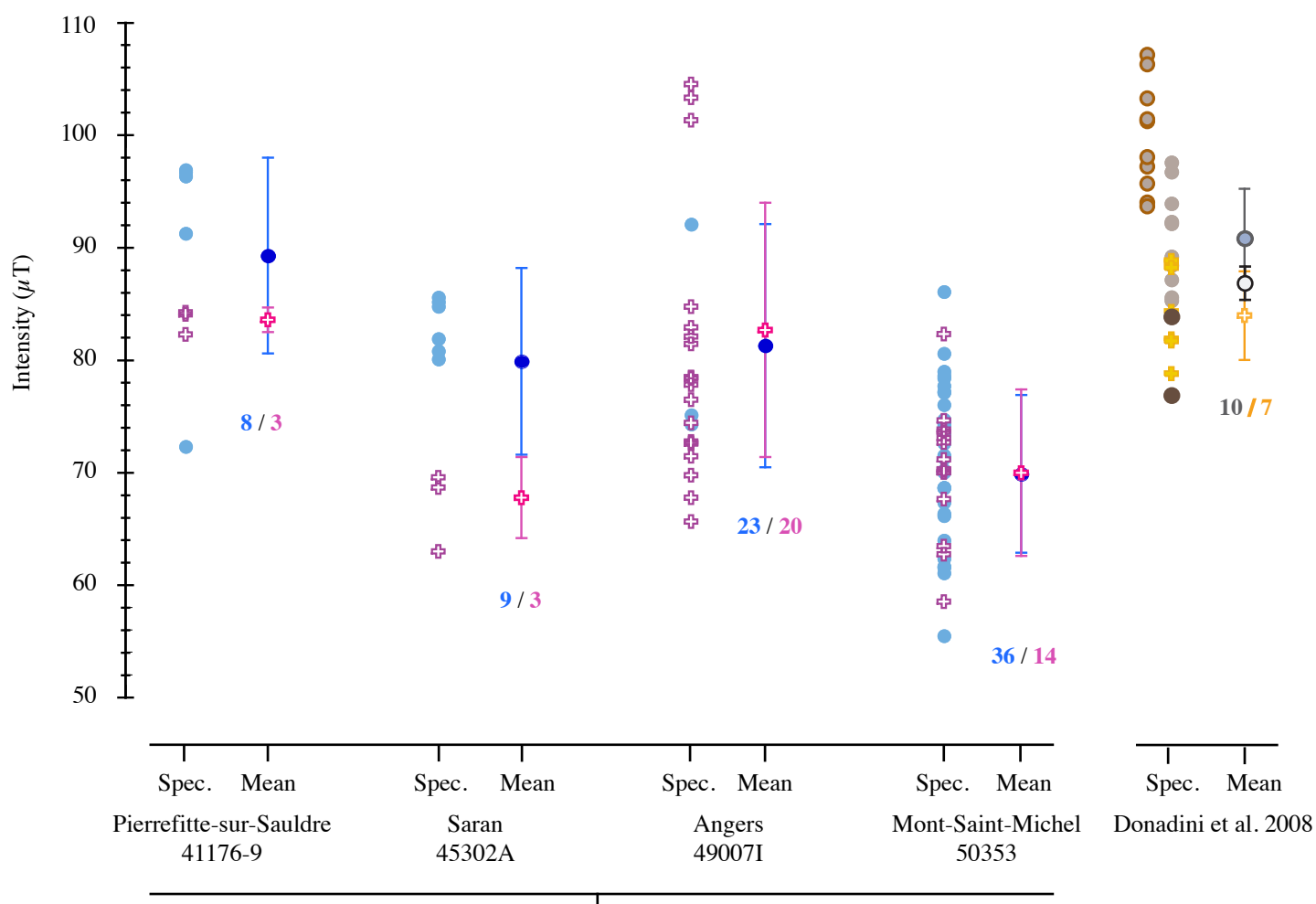
Figure 9.

Table 1

# Group	Site (Location, Archeological excavation)	Archeological description	Type of material	Age (AD.)	N Thermal unit(s) (n specimens)	F $\pm$ $\sigma$ F ( $\mu$ T)	F Beaune ( $\mu$ T)
► Groups analyzed to provide new reference intensity values							
SAR19	Saran, La Guignace (47.9°N, 1.9°E)	Kiln 10 ( SU 2761)	Potsherd	[550-620]	N=12 (n=26)	77.1 $\pm$ 2.8	76.4
SAR21	Saran, La Guignace (47.9°N, 1.9°E)	Kiln 5 (SU 2064)	Potsherd	[600-650]	N=5 (n=16)	77.7 $\pm$ 2.4	77.0
VAN03	Vanves, rue Gaudray (48.83°N, 2.30°E)	Kiln 3039 (SU 3304 & SU 3305)	Potsherd	[650-700]	N=4 (n=10)	76.9 $\pm$ 1.1	75.5
VAN09	Vanves, rue Gaudray (48.83°N, 2.30°E)	Kiln 1138 (SU 1141)	Potsherd	[650-700]	N=4 (n=9)	75.8 $\pm$ 1.3	74.5
CHAM03	Chamigny, La Grande Maison (48.97°N, 3.15°E)	Kiln 2629 (Structure 2116)	Potsherd	[675-725]	N=4 (n=15)	72.7 $\pm$ 0.9	71.3
SAR36	Saran, Voie Nouvelle (47.9°N, 1.9°E)	F 24 (SU 1073)	Potsherd	[700-750]	N=4 (n=12)	74.7 $\pm$ 2.2	74.1
HERME04	Hermé, Les Malletons carrière SPM (48.5°N, 3.3°E)	Kiln 3060; fragments from the central (and elongated) support of the floor in the firing chamber	Baked clay fragment	[970-1000]	N=1 (n=15)	62.5 $\pm$ 2.4	61.6
► Groups analyzed for dating							
BOUR01/02	La Chapelle Saint-Ursin, L'angoulaire, chemin des vallées aux fruscades (47.08°N, 2.4°E)	Kiln 3004 (SU 30121 & SU 30145)	Potsherd		N=4 (n=13)	73.2 $\pm$ 2.9	73.2
BOUR03	La Chapelle Saint-Ursin, L'angoulaire, chemin des vallées aux fruscades (47.08°N, 2.4°E)	Kiln 3004, fragments from the kiln floor in the firing chamber	Baked clay fragment		N=1 (n=11)	73.9 $\pm$ 2.2	73.9
BOUR01/02/03	La Chapelle Saint-Ursin, L'angoulaire, chemin des vallées aux fruscades (47.08°N, 2.4°E)				N=5 (n=24)	73.7 $\pm$ 2.3	73.7
CHAU01/02	Viennes-en-Arthies, Chaudry (49.07°N, 1.73°E)	Filling unit of the kiln	Potsherd		N=4 (n=12)	77.3 $\pm$ 0.5	75.8
CHAU03	Viennes-en-Arthies, Chaudry (49.07°N, 1.73°E)	Pottery fragments associated with debris of the kiln walls	Potsherd		N=2 (n=6)	77.6 $\pm$ 0.3	76.1
CHAU01/02/03	Viennes-en-Arthies, Chaudry (49.07°N, 1.73°E)				N=6 (n=18)	77.4 $\pm$ 0.4	75.9

Table 2

	Archeointensity correlation dating		Archeointensity marginalized dating	
	Our dataset	All selected data	Our dataset	All selected data
► <i>BOUR01/02/03</i> : $73.7 \pm 2.3 \mu T$				
Bootstrap algorithm Thébault and Gallet (2010)	[513 – 930]	[513 – 935]	X	X
AH-RJMCMC method Livermore et al. (2018)	[502 – 824] & [839– 926]	[508 – 583] & [640– 932]	[505 – 826] & [844 – 926]	[509 – 587] & [642 – 933]
► <i>CHAU01/02/03</i> : $75.9 \pm 0.4 \mu T$				
Bootstrap algorithm Thébault and Gallet (2010)	[543 – 895]	[543 – 905]	X	X
AH-RJMCMC method Livermore et al. (2018)	[541 – 683] & [752 – 899]	[544 – 586] & [643 – 683] & [740 – 902]	[543 – 686] & [752 – 899]	[545 – 589] & [642 – 685] & [742 – 907]
► <i>CHAU01/02/03</i> : $75.9 \pm 1.5 \mu T$				
Bootstrap algorithm Thébault and Gallet (2010)	[538 – 905]	[538 – 915]	X	X
AH-RJMCMC method Livermore et al. (2018)	[535 – 707] & [731 – 905]	[535 – 595] & [628 – 698] & [722 – 911]	[535 – 708] & [732 – 905]	[536 – 598] & [631 – 700] & [720 – 913]



Gómez-Paccard et al. 2012

Gómez-Paccard et al. 2012

=> Specimen level

- Non corrected
- + Corrected

from cooling rate effect

=> Mean level

- site/group weighted mean computed by Gomez-Paccard et al. 2012 (mixing fragments corrected and non corrected from cooling rate effect)

- + site/group weighted mean computed using only fragments for which cooling rate effect was corrected

Donadini et al. 2008

=> Specimen level

- Mini samples
- Mini samples + 10% arbitrary cooling rate effect
- Big samples
- + Big samples Sofia lab. (no fan)

Helsinki lab.

=> Mean level

- Weighted mean and weighted error computed by Donadini et al. 2008
- Mean from the mini samples values, + 10% arbitrary cooling rate effect
- + Mean derived from values obtained for the big samples analyzed in Sofia

Supp. Figure1



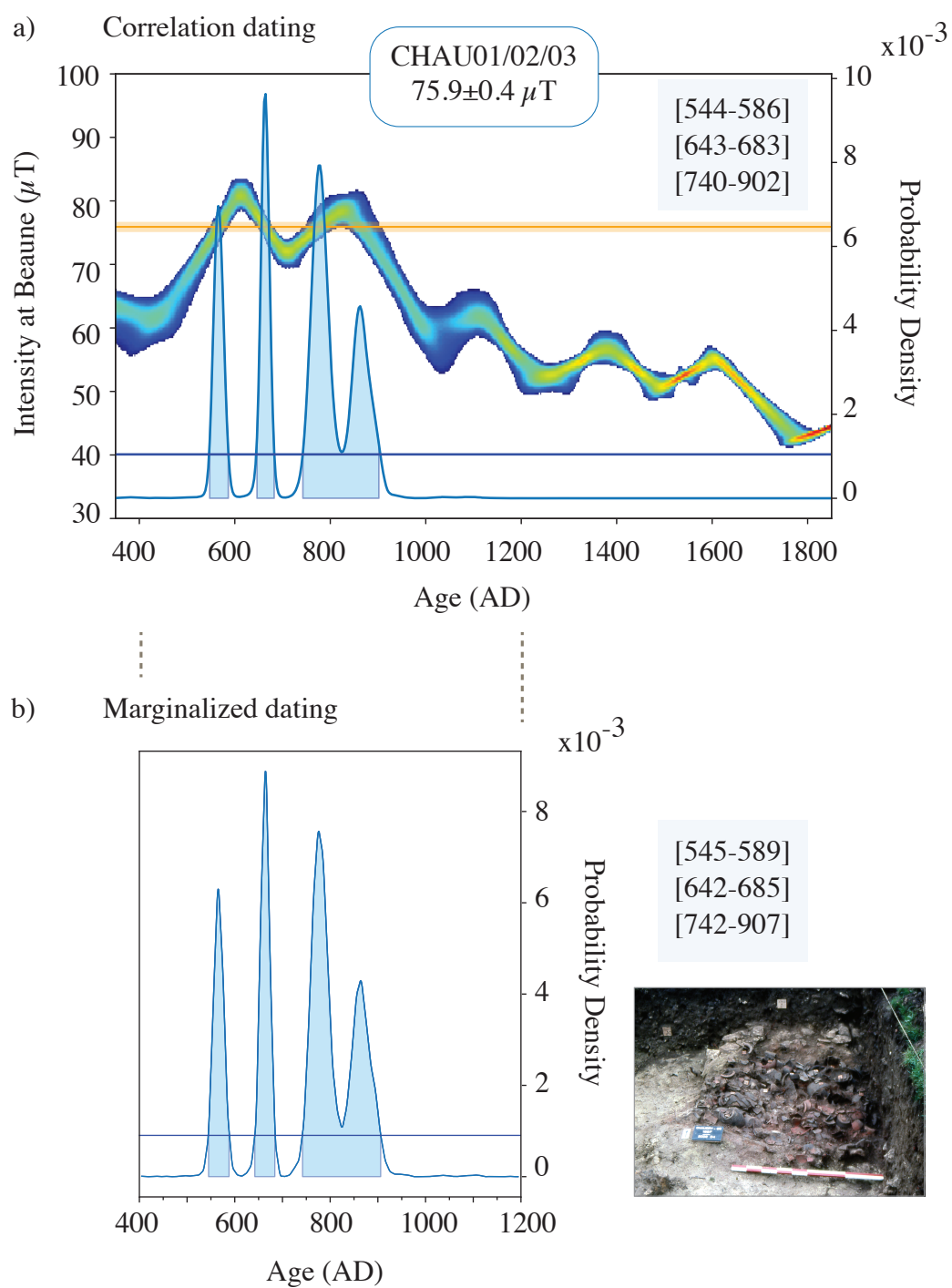


Figure S2.

Supp. Table 1

Fragment	Specimen	Natural magnetic moment	Tmin-Tmax	F Lab	NRM T1 (T1')	Slope R'	F Triaxe	F Triaxe mean value per fragment ± σF
		10 <sup>-8</sup> A.m <sup>2</sup>	(°C)	(μT)	(%)	(%)	(μT)	(μT)
SAR19, Saran - La Guignace [550-620] AD, (23/20/18/12)*, (42/26)**								
SAR19-02	SAR19-02A	52	315-495	75	87	0	80.7	80.2±0.5
	SAR19-02B	85	350-495	75	89	1	79.6	
SAR19-04	SAR19-04A	43	210-495	75	88	0	78.4	78.9±0.5
	SAR19-04C	49	180-485	75	86	-2	79.4	
SAR19-05	SAR19-05A	49	195-495	75	89	0	78.3	76.4±1.4
	SAR19-05B	37	180-485	75	86	0	75.5	
SAR19-06	SAR19-06A	87	180-495	75	94	-3	76.3	74.8±1.7
	SAR19-06B	94	180-485	75	90	6	74.1	
	SAR19-06C	101	180-485	75	92	1	72.8	
	SAR19-06D	71	180-470	75	84	-2	76.1	
SAR19-07	SAR19-07A	102	180-495	75	90	-1	74.6	76.2±1.6
	SAR19-07B	116	180-485	75	91	-2	77.8	
SAR19-12	SAR19-12A	54	180-495	75	90	3	72.8	72.5±0.4
	SAR19-12B	59	175-480	75	90	3	72.1	
SAR19-13	SAR19-13A	122	180-485	75	91	4	76.0	76.7±0.7
	SAR19-13B	130	180-475	75	89	5	77.3	
SAR19-14	SAR19-14A	117	225-485	75	80	5	75.1	74.6±0.5
	SAR19-14B	96	235-485	75	86	3	74.1	
SAR19-16	SAR19-16A	268	180-485	75	91	1	78.6	78.2±0.4
	SAR19-16B	227	180-470	75	88	1	77.7	
SAR19-18	SAR19-18A	67	265-485	75	86	-6	74.6	75.3±0.7
	SAR19-18B	69	245-490	75	84	1	76.0	
SAR19-21	SAR19-21A	200	180-485	75	78	4	82.1	82.6±0.5
	SAR19-21B	195	180-485	75	81	-2	83.1	
SAR19-23	SAR19-23A	212	180-485	75	91	-2	77.9	78.4±0.5
	SAR19-23C	210	190-470	75	86	-3	78.9	
SAR21, Saran - La Guignace [600-650] AD, (16/10/10/5)*, (28/16)**								
SAR21-02	SAR21-02A	73	200-495	75	92	4	78.3	77.8±1.1
	SAR21-02B	65	200-495	75	79	1	76.5	
	SAR21-02C	57	180-490	75	84	0	78.6	
SAR21-03	SAR21-03A	72	260-495	75	90	6	74.6	76.0±1.3
	SAR21-03B	50	260-495	75	83	0	77.3	
SAR21-05	SAR21-05B	62	220-505	75	83	2	77.6	76.1±2.1
	SAR21-05C	71	190-495	75	90	3	73.7	
	SAR21-05E	95	200-505	75	91	-1	77.0	
SAR21-11	SAR21-11A	52	180-480	75	80	5	80.8	81.7±1.9
	SAR21-11B	61	180-485	75	85	1	84.6	
	SAR21-11C	37	205-485	75	81	1	80.5	
	SAR21-11D	40	195-480	75	90	-3	80.9	
SAR21-15	SAR21-15A	43	280-480	75	71	-6	76.4	77.0±1.3
	SAR21-15B	39	265-505	75	80	-4	77.5	
	SAR21-15C	47	270-505	75	79	3	78.4	
	SAR21-15D	50	270-505	75	81	0	75.5	

**VAN03, Vanves - rue Gaudray [650-700] AD, (13/11/10/4)\*, (25/10)\*\***

VAN03-23	VAN03-23A	547	265-510	75	99	4	76.7	77.7±1.0
	VAN03-23B	668	265-490	75	98	4	78.7	
VAN03-28	VAN03-28A	145	285-490	75	90	7	77.1	77.6±1.2
	VAN03-28C	138	260-475	75	81	4	79.0	
VAN03-30	VAN03-28D	115	275-490	75	84	6	76.7	77.1±0.5
	VAN03-30A	134	225-490	75	86	5	77.5	
	VAN03-30D	95	200-500	75	81	1	76.6	
VAN03-31	VAN03-31B	56	175-485	75	78	0	76.1	75.3±0.7
	VAN03-31C	75	180-500	75	82	5	75.1	
	VAN03-31D	84	190-500	75	79	3	74.8	

**VAN09, Vanves - rue Gaudray [650-700] AD, (11/11/10/4)\*, (22/9)\*\***

VAN09-06	VAN09-06A	65	250-510	75	90	3	75.7	75.9±0.2
	VAN09-06C	60	250-500	75	80	3	76.1	
VAN09-07	VAN09-07A	103	185-510	75	94	1	76.3	75.9±0.4
	VAN09-07B	90	175-495	75	91	3	75.5	
VAN09-08	VAN09-08A	161	195-510	75	95	5	76.0	77.3±1.3
	VAN09-08B	108	175-495	75	94	1	78.6	
VAN09-11	VAN09-11A	89	175-510	75	91	7	73.5	74.1±0.7
	VAN09-11B	94	175-495	75	85	-4	74.9	
	VAN09-11C	52	175-495	75	81	3	74.0	

**CHAM03, Chamigny - La Grande Maison [675-725] AD, (19/12/9/4)\*, (24/15)\*\***

CHAM03-03	CHAM03-03A	70	275-525	75	73	3	73.2	73.7±1.3
	CHAM03-03B	131	250-515	75	73	8	75	
	CHAM03-03C	89	255-525	75	78	5	72.1	
	CHAM03-03D	126	250-510	75	72	4	74.3	
CHAM03-09	CHAM03-09B	319	285-525	75	85	4	69.6	71.8±1.8
	CHAM03-09D	191	235-515	75	82	-3	72.3	
	CHAM03-09E	257	250-515	75	91	4	73.9	
	CHAM03-09F	204	280-505	75	75	5	71.3	
CHAM03-10	CHAM03-10A	36	290-520	75	78	3	72.8	73.1±1.0
	CHAM03-10B	34	290-515	75	75	0	74.3	
	CHAM03-10D	39	280-515	75	80	6	72.3	
CHAM03-18	CHAM03-18A	67	190-520	75	89	3	71.6	72.2±0.5
	CHAM03-18B	76	195-500	75	85	1	72.5	
	CHAM03-18D	47	190-500	75	84	-6	72.6	
	CHAM03-18E	66	180-500	75	84	5	72.2	

**SAR36, Saran - Voie nouvelle [700-750] AD, (12/7/7/4)\*, (30/12)\*\***

SAR36-01	SAR36-01A	41	175-500	75	92	1	72.5	72.3±1.1
	SAR36-01B	32	180-485	75	88	-5	73.3	
	SAR36-01C	37	180-485	75	86	-2	71.2	
SAR36-08	SAR36-08A	48	245-500	75	92	9	73.5	73.4±1.2
	SAR36-08B	43	225-500	75	89	8	72.2	
	SAR36-08C	39	175-500	75	90	-7	74.5	
SAR36-12	SAR36-12A	39	340-500	75	85	5	75.7	76.5±0.7
	SAR36-12B	155	340-500	75	86	3	76.9	
	SAR36-12D	69	330-500	75	89	3	76.9	
SAR36-13	SAR36-13A	120	175-500	75	87	2	76.4	76.5±0.6
	SAR36-13B	68	185-490	75	78	0	77.1	
	SAR36-13C	42	190-500	75	89	2	76.0	

**HERME04, Hermé - Les Malletons carrière SPM [970-1000] AD, (30/15)\*\***

HERME04-01A	76	215-490	65	66	-1	66.8
HERME04-01B	143	220-515	65	84	-2	60.4
HERME04-01C	145	200-495	60	75	7	66.6
HERME04-01D	61	200-515	60	74	-7	62.9
HERME04-02A	74	185-500	65	73	-2	60.8
HERME04-02B	56	200-515	65	76	-3	60.5
HERME04-02E	61	180-500	60	75	-3	60.7
HERME04-03A	113	195-505	65	74	-2	64.7
HERME04-03B	82	205-510	65	76	-6	62.5
HERME04-04A	91	225-520	65	82	0	63.3
HERME04-04C	103	175-520	65	79	-1	65.5
HERME04-06A	145	210-520	65	76	-4	60.3
HERME04-06B	129	220-515	65	74	-5	59.9
HERME04-06C	110	235-520	60	69	3	61.3
HERME04-06D	98	205-515	60	66	0	61.8

**BOUR01/02, La Chapelle Saint-Ursin, L'angoulaire, chemin des vallées aux fruscades, (26/20/17/4)\*, (29/13)\*\***

BOUR01-05	BOUR01-05A	243	175-475	70	88	-1	74.0	74.1±0.3
	BOUR01-05C	135	185-475	75	93	0	74.4	
	BOUR01-05E	227	195-475	75	93	-1	73.9	
BOUR02-03	BOUR02-03A	743	225-485	75	57	-1	74.8	73.6±1.1
	BOUR02-03B	515	225-510	75	86	-2	73.5	
	BOUR02-03D	479	225-490	75	58	-1	72.6	
BOUR02-05	BOUR02-05A	702	175-505	75	94	-4	75.5	75.8±2.6
	BOUR02-05B	610	175-500	75	84	-1	78.3	
	BOUR02-05C	449	175-495	75	94	-3	72.2	
	BOUR02-05D	646	195-495	75	76	-1	77.1	
BOUR02-07	BOUR02-07A	785	175-495	75	66	-2	69.8	69.1±0.8
	BOUR02-07B	805	175-510	75	75	4	68.2	
	BOUR02-07C	810	175-500	75	81	-1	69.3	

**BOUR03, La Chapelle Saint-Ursin, L'angoulaire, chemin des vallées aux fruscades, (33/11)\*\***

BOUR03-01A	236	180-500	75	68	3	72.3
BOUR03-01D	172	190-490	75	82	-7	74.2
BOUR03-02A	265	180-500	75	88	-1	74.4
BOUR03-02B	318	175-525	75	94	-3	75.7
BOUR03-03A	143	175-505	75	72	-1	69.2
BOUR03-03C	380	180-490	75	81	-1	75.5
BOUR03-03G	200	150-490	75	68	1	75.2
BOUR03-08A	175	175-500	75	66	5	75.0
BOUR03-08C	120	180-490	75	79	-2	76.9
BOUR03-10B	550	160-490	75	59	-5	72.8
BOUR03-10C	200	180-490	75	79	-8	72.2

**CHAU01/02, Viennes-en-Arthies - Chaudry, (25/25/24/4)\*, (48/12)\*\***

CHAU01-01	CHAU01-01A	891	175-515	75	90	2	76.7	77.7±0.8
	CHAU01-01B	900	180-505	75	83	3	78.2	
	CHAU01-01C	840	180-505	75	83	1	78.1	
CHAU01-03	CHAU01-03A	438	385-500	75	80	2	76.0	76.8±1.4
	CHAU01-03C	342	385-505	75	88	6	76.0	
	CHAU01-03D	496	365-495	75	81	-2	78.4	
CHAU01-12	CHAU01-12A	751	180-525	75	97	2	78.3	77.7±1.1
	CHAU01-12B	840	180-505	75	92	-1	78.4	
	CHAU01-12C	658	185-505	75	93	-2	76.5	
CHAU02-08	CHAU02-08B	385	180-515	75	95	-1	76.8	77.0±0.3
	CHAU02-08C	441	180-505	75	89	0	76.8	
	CHAU02-08D	316	180-495	75	88	-3	77.3	

**CHAU03, Viennes-en-Arthies - Chaudry, (12/11/9/2)\*, (20/6)\*\***

CHAU03-05	CHAU03-05A	85	180-530	75	81	3	77.1	77.8±0.9
	CHAU03-05B	276	180-525	75	88	0	78.9	
	CHAU03-05C	123	175-505	75	73	3	77.5	
CHAU03-08	CHAU03-08A	87	180-535	75	81	-6	77.7	77.3±0.3
	CHAU03-08B	42	185-525	75	70	2	77.1	
	CHAU03-08C	124	210-525	75	83	3	77.2	

Supp. Table 2

Bootstrap algorithm							Transdimensional bayesian technique								
Fig. 6a				Fig. 6b			Fig. 6c					Fig. 6d			
Age (AD)	Probability Maximum ( $\mu$ T)	Lower Limit ( $\mu$ T)	Upper Limit ( $\mu$ T)	Probability Maximum ( $\mu$ T)	Lower Limit ( $\mu$ T)	Upper Limit ( $\mu$ T)	Age (AD)	Probability Maximum ( $\mu$ T)	Median ( $\mu$ T)	Lower Limit ( $\mu$ T)	Upper Limit ( $\mu$ T)	Probability Maximum ( $\mu$ T)	Median ( $\mu$ T)	Lower Limit ( $\mu$ T)	Upper Limit ( $\mu$ T)
300.00				66.70	74.87	58.61	298.02	52.85	57.65	44.91	81.16	65.45	66.05	59.76	76.93
303.00				66.38	73.99	58.77	301.03	53.15	57.65	45.58	79.92	65.75	66.05	60.24	75.73
306.00				66.04	73.13	58.94	304.03	53.75	57.65	46.24	78.68	65.15	65.75	60.50	74.58
309.00				65.68	72.29	59.07	307.03	54.65	57.65	46.82	77.44	65.45	65.45	60.60	73.51
312.00				65.30	71.45	59.14	310.04	54.05	57.65	47.41	76.22	65.15	65.15	60.56	72.46
315.00				64.91	70.65	59.17	313.04	54.35	57.65	47.96	74.96	64.85	65.15	60.43	71.46
318.00				64.53	69.93	59.13	316.05	54.65	57.95	48.48	73.62	64.85	64.85	60.20	70.55
321.00				64.16	69.31	59.02	319.05	55.85	57.95	49.00	72.30	64.55	64.55	59.90	69.70
324.00				63.78	68.79	58.75	322.05	55.85	57.95	49.49	70.94	64.55	64.25	59.54	68.97
327.00				63.42	68.44	58.41	325.06	56.75	57.95	49.98	69.64	64.25	64.25	59.07	68.35
330.00				63.09	68.19	57.98	328.06	56.75	58.25	50.42	68.50	64.25	63.95	58.54	67.87
333.00				62.80	68.06	57.55	331.06	57.35	58.25	50.82	67.63	63.95	63.65	57.96	67.48
336.00				62.54	67.96	57.12	334.07	57.35	58.25	51.13	66.98	63.95	63.65	57.36	67.17
339.00				62.30	67.89	56.71	337.07	57.65	58.25	51.38	66.58	63.95	63.35	56.75	66.95
342.00				62.09	67.83	56.35	340.08	57.65	58.25	51.57	66.36	63.95	63.05	56.10	66.78
345.00				61.91	67.77	56.04	343.08	57.95	58.25	51.66	66.29	63.65	63.05	55.45	66.66
348.00				61.76	67.72	55.79	346.08	57.95	58.25	51.66	66.36	63.65	62.75	54.80	66.58
351.00	60.18	54.39	65.99	61.64	67.66	55.61	349.09	58.25	58.55	51.63	66.53	63.65	62.75	54.16	66.51
354.00	60.37	54.75	65.99	61.55	67.61	55.48	352.09	58.55	58.55	51.51	66.91	63.65	62.45	53.57	66.50
357.00	60.56	55.06	66.06	61.49	67.56	55.41	355.09	58.55	58.55	51.34	67.42	63.35	62.45	53.03	66.49
360.00	60.74	55.32	66.15	61.45	67.52	55.38	358.10	58.55	58.55	51.21	67.98	63.05	62.45	52.61	66.53
363.00	60.91	55.53	66.29	61.42	67.46	55.39	361.10	59.15	58.85	51.10	68.54	63.35	62.15	52.26	66.57
366.00	61.06	55.68	66.44	61.42	67.43	55.41	364.11	58.55	58.85	51.09	69.01	63.05	62.15	52.01	66.61
369.00	61.21	55.80	66.62	61.45	67.42	55.48	367.11	58.85	59.15	51.12	69.45	63.05	62.15	51.86	66.64
372.00	61.35	55.88	66.81	61.50	67.43	55.58	370.11	59.15	59.15	51.22	69.73	62.75	61.85	51.80	66.71
375.00	61.49	55.95	67.02	61.57	67.45	55.69	373.12	59.15	59.45	51.39	70.02	62.75	61.85	51.79	66.81
378.00	61.63	56.01	67.25	61.62	67.47	55.78	376.12	59.45	59.45	51.67	70.10	62.75	61.85	51.86	66.83
381.00	61.75	56.05	67.46	61.68	67.49	55.87	379.12	59.75	59.75	52.00	70.09	62.75	61.55	52.01	66.88
384.00	61.86	56.07	67.65	61.74	67.53	55.96	382.13	60.05	59.75	52.37	69.99	62.75	61.55	52.20	66.89
387.00	61.96	56.09	67.82	61.81	67.58	56.05	385.13	60.05	60.05	52.79	69.76	62.45	61.55	52.47	66.84
390.00	62.03	56.11	67.96	61.88	67.63	56.13	388.14	60.35	60.05	53.21	69.42	62.45	61.25	52.80	66.75
393.00	62.10	56.14	68.06	61.93	67.67	56.19	391.14	60.35	60.35	53.66	68.97	62.45	61.25	53.17	66.62
396.00	62.16	56.18	68.13	61.98	67.70	56.26	394.14	60.35	60.35	54.12	68.39	62.15	61.25	53.57	66.47
399.00	62.19	56.23	68.15	62.02	67.72	56.33	397.15	60.35	60.65	54.60	67.81	62.15	61.25	53.99	66.26
402.00	62.21	56.29	68.13	62.06	67.71	56.40	400.15	60.65	60.65	55.04	67.21	61.85	61.25	54.41	66.05
405.00	62.21	56.36	68.07	62.08	67.68	56.48	403.15	61.25	60.95	55.45	66.74	61.85	61.25	54.81	65.89
408.00	62.20	56.46	67.94	62.08	67.61	56.56	406.16	61.25	60.95	55.82	66.40	61.85	61.25	55.20	65.75
411.00	62.16	56.56	67.76	62.06	67.48	56.65	409.16	61.55	61.25	56.13	66.14	61.85	61.25	55.52	65.64
414.00	62.10	56.67	67.53	62.02	67.30	56.74	412.17	61.55	61.25	56.37	65.98	61.85	61.25	55.78	65.57
417.00	62.03	56.80	67.26	61.96	67.09	56.84	415.17	61.85	61.55	56.56	65.90	61.55	61.25	55.99	65.52
420.00	61.94	56.93	66.96	61.89	66.84	56.94	418.17	62.15	61.55	56.72	65.89	61.55	61.25	56.13	65.47
423.00	61.84	57.03	66.65	61.80	66.56	57.03	421.18	62.15	61.85	56.84	65.92	61.55	61.25	56.23	65.45
426.00	61.72	57.12	66.33	61.70	66.30	57.10	424.18	62.15	61.85	56.89	66.02	61.25	61.25	56.27	65.46
429.00	61.61	57.16	66.06	61.60	66.05	57.16	427.18	62.45	62.15	56.92	66.16	61.55	61.25	56.27	65.51
432.00	61.50	57.17	65.82	61.51	65.84	57.16	430.19	62.75	62.15	56.92	66.33	61.55	61.25	56.27	65.57
435.00	61.40	57.15	65.66	61.42	65.69	57.15	433.19	63.05	62.45	56.95	66.50	61.25	61.55	56.27	65.65
438.00	61.31	57.06	65.56	61.33	65.59	57.08	436.20	63.05	62.75	56.99	66.66	61.55	61.55	56.32	65.73
441.00	61.23	56.93	65.56	61.25	65.57	56.95	439.20	63.65	62.75	57.08	66.83	61.85	61.55	56.40	65.83
444.00	61.17	56.76	65.57	61.18	65.60	56.78	442.20	63.65	63.05	57.16	67.00	61.85	61.85	56.49	65.95
447.00	61.12	56.56	65.68	61.13	65.67	56.59	445.21	64.25	63.35	57.25	67.18	62.15	61.85	56.63	66.09
450.00	61.10	56.65	65.82	61.09	65.81	56.38	448.21	64.25	63.35	57.31	67.38	62.15	62.15	56.73	66.26
453.00	61.09	56.15	66.02	61.11	66.00	56.20	451.21	64.85	63.65	57.38	67.59	62.15	62.15	56.84	66.45
456.00	61.12	55.99	66.24	61.15	66.24	56.06	454.22	65.15	63.95	57.43	67.80	62.15	62.45	56.93	66.66
459.00	61.20	55.90	66.50	61.24	66.51	55.96	457.22	65.45	64.25	57.48	68.03	63.05	62.45	57.04	66.88
462.00	61.31	55.86	66.78	61.36	66.80	55.95	460.23	65.75	64.55	57.48	68.26	63.35	62.75	57.13	67.13
465.00	61.47	55.87	67.06	61.53	67.10	55.96	463.23	66.05	64.85	57.50	68.51	63.65	63.05	57.19	67.38
468.00	61.66	55.96	67.35	61.73	67.42	56.05	466.23	66.35	65.15	57.50	68.77	63.95	63.35	57.25	67.64
471.00	61.90	56.11	67.68	61.98	67.76	56.21	469.24	66.65	65.45	57.48	69.03	64.55	63.65	57.29	67.91
474.00	62.18	56.34	68.02	62.29	68.13	56.45	472.24	66.95	65.75	57.45	69.30	64.85	63.95	57.31	68.20
477.00	62.50	56.62	68.39	62.60	68.50	56.71	475.24								

597.00	77.26	74.63	79.91	77.82	81.35	74.31	595.39	77.45	77.75	75.98	80.08	79.25	79.85	77.05	83.23
600.00	77.25	74.54	79.94	77.91	81.54	74.28	598.40	77.45	77.75	76.06	80.18	79.85	80.15	77.36	83.42
603.00	77.22	74.49	79.94	77.99	81.63	74.34	601.40	77.75	77.75	76.11	80.27	80.45	80.45	77.66	83.56
606.00	77.18	74.46	79.91	78.05	81.68	74.42	604.40	77.45	77.75	76.12	80.34	80.75	80.75	77.95	83.69
609.00	77.15	74.45	79.85	78.11	81.72	74.48	607.41	77.45	77.75	76.10	80.39	80.75	80.75	78.21	83.78
612.00	77.10	74.40	79.79	78.11	81.77	74.45	610.41	77.45	77.75	76.07	80.42	80.75	80.75	78.39	83.84
615.00	77.04	74.32	79.76	78.09	81.84	74.33	613.42	77.15	77.75	76.02	80.43	80.75	81.05	78.45	83.87
618.00	76.97	74.21	79.74	78.02	81.88	74.15	616.42	77.15	77.75	75.96	80.41	80.75	80.75	78.37	83.87
621.00	76.91	74.11	79.71	77.94	81.89	74.00	619.42	76.85	77.45	75.90	80.38	80.75	80.75	78.20	83.84
624.00	76.85	74.04	79.67	77.85	81.79	73.90	622.43	76.85	77.45	75.83	80.30	80.45	80.75	77.96	83.78
627.00	76.78	74.01	79.56	77.76	81.62	73.92	625.43	76.85	77.15	75.75	80.20	80.15	80.45	77.71	83.67
630.00	76.70	74.00	79.41	77.66	81.34	73.98	628.43	76.85	77.15	75.66	80.06	79.55	80.15	77.46	83.51
633.00	76.62	74.01	79.23	77.53	81.02	74.05	631.44	76.55	77.15	75.57	79.90	79.25	79.85	77.22	83.34
636.00	76.54	74.01	79.07	77.39	80.70	74.08	634.44	76.55	76.85	75.48	79.69	78.95	79.25	76.98	83.11
639.00	76.45	73.97	78.94	77.24	80.41	74.06	637.45	76.55	76.85	75.37	79.45	78.65	78.95	76.75	82.83
642.00	76.37	73.89	78.84	77.06	80.14	73.99	640.45	76.25	76.55	75.27	79.19	78.35	78.65	76.51	82.46
645.00	76.28	73.81	78.75	76.87	79.90	73.84	643.45	76.25	76.55	75.15	78.89	78.05	78.35	76.27	81.98
648.00	76.20	73.74	78.66	76.68	79.65	73.69	646.46	76.25	76.25	75.03	78.58	77.75	78.05	76.03	81.42
651.00	76.12	73.74	78.51	76.49	79.38	73.61	649.46	75.95	76.25	74.91	78.29	77.45	77.45	75.76	80.78
654.00	76.04	73.75	78.32	76.32	79.05	73.59	652.46	75.95	75.95	74.78	78.00	77.15	77.15	75.47	80.11
657.00	75.95	73.78	78.11	76.16	78.72	73.59	655.47	75.65	75.95	74.63	77.74	76.85	76.85	75.15	79.47
660.00	75.88	73.78	77.99	76.01	78.44	73.59	658.47	75.65	75.65	74.48	77.49	76.25	76.55	74.78	78.88
663.00	75.80	73.68	77.93	75.87	78.25	73.50	661.48	75.35	75.65	74.30	77.26	76.25	76.25	74.36	78.34
666.00	75.72	73.61	77.95	75.72	78.14	73.31	664.48	75.35	75.35	74.11	77.06	75.95	75.95	73.88	77.84
669.00	75.63	73.26	78.00	75.54	78.08	73.01	667.48	75.05	75.05	73.88	76.88	75.35	75.35	73.36	77.39
672.00	75.50	73.22	77.99	75.33	77.98	72.68	670.49	75.05	75.05	73.62	76.71	75.05	75.05	72.80	76.97
675.00	75.34	72.74	77.95	75.09	77.84	72.33	673.49	74.75	74.75	73.33	76.56	75.05	74.75	72.22	76.59
678.00	75.12	72.51	77.74	74.81	77.59	72.04	676.49	74.75	74.75	72.99	76.40	74.75	74.45	71.66	76.24
681.00	74.89	72.28	77.49	74.51	77.27	71.74	679.50	74.45	74.45	72.61	76.25	74.45	74.15	71.18	75.92
684.00	74.63	72.03	77.23	74.18	76.94	71.41	682.50	74.45	74.15	72.22	76.08	74.15	73.85	70.77	75.60
687.00	74.36	71.70	77.02	73.87	76.68	71.05	685.51	74.15	74.15	71.86	75.89	73.85	73.55	70.43	75.30
690.00	74.09	71.32	76.87	73.57	76.49	70.65	688.51	73.85	73.85	71.52	75.68	73.55	72.95	70.13	75.01
693.00	73.82	70.87	76.77	73.27	76.34	70.19	691.51	73.85	73.85	71.25	75.45	73.25	72.65	69.90	74.74
696.00	73.56	70.45	76.67	72.98	76.20	69.77	694.52	73.55	73.55	71.03	75.21	72.65	72.65	69.71	74.47
699.00	73.33	70.08	76.57	72.74	76.06	69.40	697.52	73.25	73.25	70.85	74.98	72.65	72.35	69.57	74.23
702.00	73.13	69.85	76.41	72.54	75.89	69.19	700.52	73.25	73.25	70.72	74.77	72.35	72.05	69.45	74.02
705.00	72.97	69.72	76.22	72.39	75.69	69.08	703.53	73.25	72.95	70.62	74.61	72.05	72.05	69.35	73.86
708.00	72.84	69.66	76.03	72.28	75.50	69.06	706.53	72.95	72.95	70.55	74.47	72.05	72.05	69.27	73.78
711.00	72.76	69.61	75.91	72.23	75.43	69.03	709.54	72.95	72.65	70.49	74.36	72.05	71.75	69.21	73.78
714.00	72.71	69.57	75.85	72.21	75.43	69.00	712.54	72.65	72.65	70.43	74.29	72.05	72.05	69.17	73.88
717.00	72.70	69.47	75.91	72.22	75.51	68.92	715.54	72.65	72.65	70.37	74.26	72.05	72.05	69.14	74.01
720.00	72.70	69.35	76.05	72.28	75.76	68.81	718.55	72.65	72.65	70.29	74.27	72.05	72.05	69.10	74.20
723.00	72.76	69.23	76.28	72.40	76.08	68.72	721.55	72.65	72.65	70.20	74.32	72.35	72.05	69.06	74.39
726.00	72.84	69.16	76.52	72.57	76.44	68.70	724.55	72.65	72.65	70.09	74.41	72.65	72.35	69.03	74.62
729.00	72.96	69.17	76.75	72.79	76.81	68.78	727.56	72.65	72.65	69.97	74.54	72.95	72.65	69.00	74.88
732.00	73.09	69.23	76.95	73.05	77.16	68.92	730.56	72.95	72.65	69.88	74.68	72.95	72.65	68.98	75.18
735.00	73.24	69.34	77.13	73.33	77.49	69.16	733.57	72.95	72.65	69.81	74.85	73.25	72.95	69.01	75.50
738.00	73.40	69.52	77.28	73.64	77.83	69.46	736.57	73.25	72.95	69.77	75.02	73.55	73.25	69.05	75.86
741.00	73.58	69.72	77.45	73.98	78.16	69.81	739.57	73.25	72.95	69.74	75.21	73.55	73.55	69.14	76.25
744.00	73.78	69.95	77.62	74.33	78.49	70.17	742.58	73.55	73.25	69.75	75.41	73.85	73.55	69.30	76.63
747.00	73.98	70.17	77.80	74.69	78.84	70.55	745.58	73.85	73.25	69.79	75.63	73.85	73.85	69.52	76.99
750.00	74.19	70.38	77.99	75.06	79.20	70.92	748.58	73.85	73.55	69.85	75.87	74.15	74.15	69.85	77.36
753.00	74.41	70.59	78.23	75.40	79.56	71.25	751.59	74.15	73.85	69.95	76.12	74.15	74.45	70.33	77.74
756.00	74.63	70.79	78.48	75.74	79.92	71.57	754.59	74.15	73.85	70.06	76.40	74.45	74.45	70.89	78.09
759.00	74.85	70.97	78.74	76.08	80.29	71.87	757.60	74.45	74.15	70.22	76.69	74.75	74.75	71.45	78.46
762.00	75.07	71.14	79.00	76.40	80.63	72.16	760.60	74.45	74.45	70.42	76.98	74.75	75.05	71.99	78.81
765.00	75.29	71.33	79.24	76.69	80.94	72.44	763.60	74.75	74.45	70.65	77.27	75.05	75.05	72.47	79.16
768.00	75.50	71.53	79.46	76.93	81.17	72.70	766.61	74.75	74.75	70.93	77.56	75.35	75.35	72.89	79.47
771.00	75.69	71.76	79.63	77.14	81.32	72.96	769.61	75.05	74.75	71.24	77.84	75.35	75.65	73.24	79.79
774.00	75.88	72.01	79.75	77.32	81.41	73.24	772.61	75.05	75.05	71.59	78.13	75.65	75.65	73.57	80.06
777.00	76.07	72.31	79.82	77.45	81.40	73.51	775.62	75.35	75.35	71.98	78.42	75.65	75.95	73.86	80.31
780.00	76.24	72.61	79.87	77.54	81.34	73.75	778.62	75.35	75.35	72.38	78.68	75.95	76.25	74.11	80.53
783.00	76.40	72.88	79.92	77.59	81.25	73.93	781.63	75.65	75.65	72.79	78.95	75.95	76.25	74.34	80.74
786.00	76.56	73.12	80.00	77.62	81.21	74.03	784.63	75.65	75.95	73.18	79.21	76.25	76.55	74.54	80.93
789.00	76.73	73.32	80.14	77.64	81.20	74.08	787.63	75.95	75.95	73.55	79.47	76.55	76.85	74.74	81.07
792.00	76.89	73.46	80.31	77.65	81.22	74.06	790.64	76.25	76.25	73.88	79.71	76.55	76.85	74.92	81.16
795.00	77.04	73.59	80.49	77.65	81.28	74.03	793.64	76.25	76.55	74.18	79.91	76.85	77.15	75.08	81.22
798.00	77.18	73.72	80.65	77.68	81.32	74.05	796.64	76.55	76.55	74.44	80.08	76.85	77.45	75.24	81.23
801.00	77.32	73.90	80.73	77.72	81.33	74.10	799.65	76.55	76.85	74.66	80.21	77.15	77.45	75.39	81.22
804.00	77.45	74.14	80.76	77.79	81.29	74.29	802.65	76.85	76.85	74.86	80.32	77.45	77.75	75.53	81.19
807.00	77.59	74.44	80.74	77.88	81.22	74.53	805.66	76.85	77.15	75.04	80.41	77.45	77.75	75.66	81.15
810.00	77.73	74.76	80.70	77.97	81.14	74.79	808.66	77.15	77.45	75.21	80.47	77.75	78.05	75.78	81.11
813.00	77.86	75.06	80.65	78.06	81.10	75.03	811.66	77.45	77.45	75.35	80.53	77.75	78.05	75.88	81.07
816.00	77.96	75.29	80.64	78.15	81.09	75.20	814.67	77.45	77.75	75.48	80.60	78.05	78.05	75.97	81.04

921.00	70.39	63.59	77.20	71.16	78.46	63.86	919.80	69.35	69.35	60.06	74.88	69.35	69.95	62.46	74.83
924.00	69.92	62.71	77.13	70.69	78.41	62.97	922.80	69.05	69.05	59.38	74.47	69.05	69.35	61.67	74.48
927.00	69.43	61.80	77.05	70.21	78.35	62.07	925.81	68.75	68.45	58.80	74.10	68.75	69.05	60.97	74.19
930.00	68.91	60.87	76.95	69.71	78.26	61.16	928.81	68.45	68.15	58.30	73.77	68.45	68.45	60.30	73.94
933.00	68.38	59.94	76.81	69.21	78.12	60.29	931.81	68.15	67.55	57.88	73.41	68.15	68.15	59.74	73.67
936.00	67.84	59.05	76.64	68.69	77.92	59.46	934.82	67.85	67.25	57.55	73.07	67.85	67.85	59.25	73.41
939.00	67.30	58.20	76.41	68.15	77.61	58.69	937.82	67.25	66.95	57.24	72.68	67.25	67.25	58.84	73.12
942.00	66.78	57.43	76.13	67.63	77.22	58.05	940.82	67.25	66.35	56.98	72.26	66.95	66.95	58.49	72.80
945.00	66.26	56.75	75.78	67.12	76.71	57.53	943.83	66.65	66.05	56.76	71.77	66.65	66.35	58.22	72.41
948.00	65.75	56.15	75.35	66.58	76.04	57.12	946.83	66.35	65.45	56.62	71.27	66.35	66.05	57.99	71.98
951.00	65.24	55.65	74.83	66.04	75.26	56.84	949.84	65.75	65.15	56.51	70.72	65.75	65.75	57.78	71.50
954.00	64.72	55.24	74.18	65.51	74.36	56.65	952.84	65.45	64.55	56.48	70.12	65.45	65.15	57.61	70.99
957.00	64.21	54.99	73.43	64.97	73.39	56.56	955.84	65.15	64.25	56.51	69.52	64.85	64.85	57.47	70.40
960.00	63.72	54.87	72.58	64.43	72.34	56.52	958.85	64.55	63.65	56.54	68.91	64.55	64.25	57.38	69.78
963.00	63.22	54.88	71.58	63.90	71.27	56.54	961.85	63.95	63.35	56.62	68.33	64.25	63.95	57.32	69.21
966.00	62.73	54.93	70.51	63.39	70.20	56.58	964.85	63.05	63.05	56.73	67.78	63.95	63.65	57.32	68.62
969.00	62.24	55.09	69.39	62.89	69.16	56.63	967.86	62.45	62.75	56.85	67.25	63.35	63.05	57.32	68.03
972.00	61.79	55.28	68.30	62.41	68.18	56.63	970.86	62.15	62.15	56.96	66.76	63.05	62.75	57.32	67.45
975.00	61.36	55.46	67.27	61.94	67.28	56.59	973.87	61.85	61.85	57.03	66.30	62.45	62.45	57.27	66.93
978.00	60.95	55.54	66.33	61.50	66.51	56.49	976.87	61.55	61.55	57.04	65.89	61.85	61.85	57.18	66.44
981.00	60.56	55.56	65.56	61.10	65.88	56.32	979.87	61.55	61.55	56.97	65.49	61.55	61.55	57.01	65.99
984.00	60.21	55.45	64.95	60.73	65.39	56.07	982.88	60.95	61.25	56.81	65.14	61.25	61.25	56.77	65.60
987.00	59.89	55.26	64.53	60.38	65.00	55.76	985.88	60.95	60.95	56.57	64.83	60.95	60.95	56.43	65.25
990.00	59.60	54.97	64.23	60.04	64.69	55.39	988.88	60.95	60.65	56.26	64.56	60.65	60.65	55.99	64.97
993.00	59.33	54.64	64.02	59.74	64.46	55.02	991.89	60.65	60.65	55.84	64.34	60.35	60.35	55.48	64.76
996.00	59.07	54.27	63.88	59.46	64.26	54.65	994.89	60.65	60.35	55.36	64.19	60.35	60.05	54.90	64.64
999.00	58.84	53.90	63.77	59.19	64.10	54.28	997.90	60.65	60.35	54.84	64.10	60.05	59.75	54.29	64.62
1002.00	58.63	53.55	63.71	58.95	63.96	53.94	1000.90	60.65	60.05	54.27	64.07	60.05	59.75	53.66	64.71
1005.00	58.44	53.23	63.65	58.73	63.85	53.61	1003.90	60.65	60.05	53.71	64.13	59.75	59.45	53.03	64.92
1008.00	58.25	52.90	63.59	58.53	63.75	53.31	1006.91	60.65	60.05	53.17	64.20	59.45	59.15	52.41	65.21
1011.00	58.08	52.61	63.55	58.35	63.68	53.03	1009.91	60.35	60.05	52.64	64.37	59.45	59.15	51.77	65.59
1014.00	57.94	52.35	63.53	58.20	63.63	52.78	1012.91	60.35	59.75	52.11	64.58	59.75	58.85	51.17	65.96
1017.00	57.82	52.13	63.53	58.08	63.63	52.55	1015.92	60.35	59.75	51.59	64.87	59.45	58.85	50.54	66.35
1020.00	57.73	51.92	63.54	57.99	63.63	52.34	1018.92	60.35	59.75	51.10	65.25	60.05	58.85	49.95	66.90
1023.00	57.66	51.75	63.58	57.91	63.67	52.15	1021.93	60.35	59.75	50.61	65.65	59.45	58.55	49.35	67.50
1026.00	57.62	51.60	63.65	57.85	63.73	51.97	1024.93	60.35	59.75	50.13	66.12	60.35	58.55	48.79	68.05
1029.00	57.60	51.46	63.74	57.80	63.81	51.80	1027.93	60.05	59.75	49.70	66.49	60.65	58.55	48.30	68.56
1032.00	57.60	51.35	63.85	57.79	63.93	51.64	1030.94	60.05	59.75	49.30	66.89	60.65	58.55	47.85	68.95
1035.00	57.62	51.25	63.99	57.79	64.07	51.51	1033.94	60.05	59.75	49.01	67.19	60.65	58.85	47.52	69.28
1038.00	57.67	51.17	64.16	57.81	64.24	51.39	1036.94	60.05	59.75	48.80	67.34	60.65	58.85	47.28	69.49
1041.00	57.73	51.12	64.35	57.86	64.43	51.30	1039.95	60.05	59.75	48.61	67.50	60.95	58.85	47.13	69.52
1044.00	57.81	51.07	64.55	57.94	64.64	51.23	1042.95	60.05	59.75	48.50	67.61	60.95	59.15	47.07	69.48
1047.00	57.92	51.07	64.77	58.03	64.86	51.22	1045.96	60.05	59.75	48.48	67.64	60.95	59.15	47.04	69.38
1050.00	58.04	51.09	65.00	58.15	65.09	51.21	1048.96	59.75	59.75	48.53	67.58	60.95	59.45	47.05	69.25
1053.00	58.18	51.14	65.22	58.27	65.31	51.23	1051.96	59.75	59.75	48.66	67.53	60.95	59.75	47.23	69.08
1056.00	58.33	51.22	65.45	58.40	65.52	51.29	1054.97	59.75	59.75	48.87	67.47	60.95	59.75	47.40	68.90
1059.00	58.51	51.36	65.67	58.56	65.72	51.40	1057.97	59.75	59.75	49.13	67.46	60.95	60.05	47.67	68.76
1062.00	58.70	51.53	65.86	58.74	65.92	51.57	1060.97	59.75	59.75	49.46	67.50	60.95	60.35	48.01	68.71
1065.00	58.89	51.74	66.03	58.95	66.10	51.79	1063.98	59.75	60.05	49.90	67.56	60.95	60.35	48.40	68.74
1068.00	59.12	52.03	66.20	59.16	66.26	52.07	1066.98	59.75	60.05	50.36	67.71	60.95	60.65	48.87	68.82
1071.00	59.36	52.38	66.34	59.39	66.38	52.40	1069.99	59.75	60.05	50.92	67.88	60.95	60.65	49.51	68.97
1074.00	59.60	52.78	66.43	59.64	66.48	52.80	1072.99	59.45	60.05	51.57	68.05	60.95	60.95	50.18	69.11
1077.00	59.87	53.25	66.48	59.89	66.52	53.26	1075.99	59.45	60.05	52.25	68.22	61.25	61.25	50.91	69.25
1080.00	60.15	53.78	66.52	60.15	66.54	53.76	1079.00	59.45	60.05	52.96	68.42	61.25	61.25	51.65	69.45
1083.00	60.43	54.34	66.51	60.43	66.54	54.31	1082.00	59.45	60.05	53.71	68.60	61.25	61.55	52.39	69.64
1086.00	60.71	54.93	66.50	60.70	66.53	54.88	1085.00	59.45	60.35	54.46	68.79	61.25	61.55	53.21	69.81
1089.00	60.99	55.51	66.47	60.98	66.50	55.46	1088.01	59.45	60.35	55.26	68.92	61.25	61.55	54.07	69.91
1092.00	61.26	56.08	66.44	61.25	66.48	56.03	1091.01	59.15	60.35	56.03	69.07	61.55	61.85	54.89	70.04
1095.00	61.53	56.63	66.43	61.51	66.46	56.56	1094.02	59.15	60.35	56.75	69.13	61.55	61.85	55.73	70.09
1098.00	61.78	57.13	66.43	61.75	66.47	57.04	1097.02	59.15	60.65	57.21	69.14	61.55	61.85	56.56	70.03
1101.00	62.02	57.57	66.46	61.98	66.48	57.48	1100.02	59.15	60.65	57.43	69.10	61.85	62.15	57.25	69.93
1104.00	62.24	57.96	66.53	62.21	66.55	57.87	1103.03	59.15	60.65	57.53	68.96	61.55	62.15	57.77	69.74
1107.00	62.43	58.26	66.61	62.41	66.64	58.18	1106.03	58.85	60.95	57.58	68.85	61.55	62.15	58.06	69.52
1110.00	62.59	58.49	66.70	62.58	66.73	58.42	1109.03	58.85	60.95	57.60	68.66	61.55	62.15	58.24	69.26
1113.00	62.71	58.64	66.78	62.70	66.81	58.60	1112.04	58.85	60.95	57.59	68.44	61.85	62.15	58.34	68.94
1116.00	62.79	58.74	66.84	62.79	66.86	58.71	1115.04	58.85	60.95	57.57	68.21	61.55	61.85	58.37	68.63
1119.00	62.84	58.82	66.86	62.84	66.87	58.79	1118.05	58.85	60.65	57.55	67.98	61.55	61.85	58.37	68.34
1122.00	62.84	58.85	66.84	62.83	66.84	58.84	1121.05	58.85	60.65	57.51	67.74	61.55	61.85	58.32	68.08
1125.00	62.78	58.86	66.71	62.80	66.72	58.87	1124.05	58.55	60.65	57.46	67.47	61.55	61.85	58.25	67.73
1128.00	62.68	58.85	66.50	62.69	66.51	58.86	1127.06	58.55	60.35	57.41	67.17	61.25	61.55	58.15	67.39
1131.00	62.51	58.81	66.20	62.53	66.22	58.83	1130.06	58.55	60.35	57.35	66.88	60.65	61.25	58.04	67.10
1134.00	62.31	58.75	65.86	62.30	65.86	58.74	1133.06	58.55	60.05	57.29	66.59	60.65	61.25	57.91	66.78
1137.00	62.06	58.64	65.48	62.04	65.47	58.61	1136.07	58.55	59.75	57.21	66.29	60.35	60.95	57.77	66.48
1140.00	61.76	58.45	65.06	61.73	65.06	58.40									



1245.00	52.60	48.55	56.65	52.52	55.86	49.17	1244.20	56.45	55.25	49.74	57.24	52.55	52.25	49.71	54.46
1248.00	52.73	48.86	56.62	52.61	55.93	49.31	1247.21	56.45	55.25	49.85	57.18	52.55	52.25	49.76	54.35
1251.00	52.87	49.14	56.61	52.71	55.95	49.46	1250.21	56.45	55.25	49.97	57.12	52.55	52.25	49.80	54.27
1254.00	53.02	49.38	56.66	52.80	55.94	49.66	1253.21	56.45	55.25	50.09	57.07	52.55	52.25	49.84	54.21
1257.00	53.16	49.57	56.75	52.88	55.93	49.84	1256.22	56.15	54.95	50.22	57.01	52.55	52.25	49.85	54.16
1260.00	53.30	49.71	56.88	52.95	55.92	49.99	1259.22	56.15	54.95	50.35	56.95	52.55	52.25	49.87	54.15
1263.00	53.43	49.82	57.04	53.02	55.96	50.07	1262.23	56.15	54.95	50.50	56.89	52.55	52.55	49.87	54.16
1266.00	53.56	49.91	57.22	53.07	56.04	50.09	1265.23	56.15	54.95	50.64	56.84	52.55	52.55	49.85	54.19
1269.00	53.67	49.97	57.38	53.10	56.18	50.02	1268.23	56.15	54.95	50.76	56.78	52.55	52.55	49.81	54.23
1272.00	53.77	50.03	57.51	53.13	56.33	49.93	1271.24	55.85	54.95	50.89	56.73	52.85	52.55	49.75	54.29
1275.00	53.86	50.12	57.61	53.16	56.48	49.85	1274.24	55.85	54.95	51.02	56.67	52.85	52.55	49.68	54.35
1278.00	53.93	50.22	57.62	53.20	56.60	49.81	1277.24	55.85	54.95	51.15	56.62	52.85	52.55	49.59	54.42
1281.00	53.97	50.33	57.61	53.25	56.69	49.81	1280.25	55.85	54.95	51.29	56.57	53.15	52.85	49.50	54.49
1284.00	54.01	50.47	57.55	53.30	56.75	49.85	1283.25	55.85	54.95	51.43	56.52	53.15	52.85	49.41	54.56
1287.00	54.04	50.62	57.45	53.34	56.76	49.92	1286.26	55.85	54.95	51.58	56.47	53.45	52.85	49.31	54.63
1290.00	54.05	50.78	57.33	53.39	56.76	50.01	1289.26	55.55	54.95	51.71	56.42	53.45	53.15	49.22	54.71
1293.00	54.07	50.95	57.19	53.44	56.75	50.13	1292.26	55.55	54.95	51.87	56.37	53.45	53.15	49.13	54.79
1296.00	54.08	51.12	57.04	53.50	56.74	50.25	1295.27	55.55	54.95	52.04	56.33	53.75	53.45	49.07	54.87
1299.00	54.10	51.29	56.90	53.56	56.73	50.39	1298.27	55.55	54.95	52.20	56.28	53.75	53.45	49.07	54.95
1302.00	54.11	51.45	56.77	53.63	56.73	50.52	1301.27	55.55	54.95	52.39	56.24	53.75	53.45	49.10	55.04
1305.00	54.13	51.60	56.66	53.70	56.74	50.66	1304.28	55.25	54.95	52.58	56.19	54.05	53.75	49.22	55.13
1308.00	54.16	51.74	56.58	53.78	56.75	50.81	1307.28	55.25	54.95	52.77	56.16	54.05	53.75	49.42	55.23
1311.00	54.21	51.88	56.54	53.88	56.77	50.99	1310.29	55.25	54.95	52.98	56.13	54.35	54.05	49.73	55.33
1314.00	54.27	52.02	56.53	53.99	56.78	51.19	1313.29	55.25	54.95	53.19	56.11	54.35	54.05	50.15	55.44
1317.00	54.35	52.17	56.52	54.10	56.78	51.43	1316.29	55.25	54.95	53.40	56.11	54.35	54.05	50.73	55.56
1320.00	54.45	52.34	56.56	54.24	56.76	51.71	1319.30	55.25	54.95	53.58	56.13	54.35	54.35	51.40	55.70
1323.00	54.57	52.54	56.60	54.40	56.75	52.05	1322.30	54.95	54.95	53.74	56.17	54.65	54.35	52.12	55.85
1326.00	54.71	52.76	56.66	54.58	56.75	52.41	1325.30	54.95	54.95	53.86	56.23	54.65	54.65	52.77	56.03
1329.00	54.88	53.01	56.74	54.77	56.81	52.76	1328.31	54.95	54.95	53.93	56.33	54.95	54.95	53.31	56.29
1332.00	55.06	53.26	56.86	54.98	56.97	52.98	1331.31	54.95	54.95	53.98	56.45	54.95	54.95	53.65	56.66
1335.00	55.25	53.49	57.03	55.20	57.31	53.09	1334.32	54.95	54.95	54.00	56.60	55.25	55.25	53.87	57.13
1338.00	55.46	53.66	57.25	55.42	57.76	53.06	1337.32	54.95	54.95	53.99	56.77	55.25	55.25	54.02	57.59
1341.00	55.66	53.79	57.54	55.63	58.27	53.00	1340.32	54.95	54.95	53.98	56.94	55.25	55.25	54.14	58.02
1344.00	55.86	53.83	57.88	55.85	58.77	52.93	1343.33	54.95	54.95	53.96	57.11	55.55	55.55	54.23	58.41
1347.00	56.04	53.84	58.24	56.05	59.18	52.94	1346.33	54.65	54.95	53.94	57.27	55.55	55.85	54.30	58.74
1350.00	56.21	53.81	58.62	56.23	59.48	52.99	1349.33	54.65	54.95	53.91	57.41	55.85	55.85	54.35	59.01
1353.00	56.36	53.76	58.97	56.39	59.62	53.14	1352.34	54.65	54.95	53.88	57.54	55.85	56.15	54.40	59.22
1356.00	56.48	53.69	59.28	56.50	59.70	53.30	1355.34	54.65	54.95	53.84	57.67	56.15	56.15	54.44	59.41
1359.00	56.57	53.62	59.51	56.58	59.74	53.43	1358.35	54.65	54.95	53.81	57.77	56.15	56.45	54.47	59.55
1362.00	56.61	53.56	59.66	56.65	59.83	53.43	1361.35	54.35	54.95	53.77	57.85	56.15	56.45	54.48	59.65
1365.00	56.62	53.51	59.74	56.68	59.99	53.38	1364.35	54.35	54.95	53.73	57.92	56.45	56.45	54.48	59.75
1368.00	56.60	53.45	59.74	56.68	60.18	53.21	1367.36	54.35	54.65	53.69	57.96	56.45	56.45	54.46	59.84
1371.00	56.52	53.39	59.65	56.67	60.36	52.98	1370.36	54.35	54.65	53.65	58.01	56.45	56.75	54.43	59.94
1374.00	56.43	53.32	59.53	56.62	60.49	52.76	1373.36	54.35	54.65	53.61	58.03	56.45	56.75	54.40	60.03
1377.00	56.31	53.25	59.36	56.54	60.50	52.55	1376.37	54.35	54.65	53.57	58.03	56.45	56.75	54.36	60.11
1380.00	56.15	53.15	59.15	56.43	60.49	52.37	1379.37	54.05	54.65	53.53	58.03	56.45	56.75	54.31	60.18
1383.00	55.97	53.02	58.92	56.30	60.39	52.21	1382.38	54.05	54.65	53.48	58.02	56.45	56.75	54.26	60.22
1386.00	55.77	52.87	58.68	56.15	60.22	52.07	1385.38	54.05	54.35	53.43	58.00	56.45	56.75	54.21	60.25
1389.00	55.57	52.69	58.45	55.98	60.02	51.94	1388.38	54.05	54.35	53.39	57.96	56.45	56.45	54.16	60.26
1392.00	55.36	52.49	58.23	55.79	59.77	51.81	1391.39	54.05	54.35	53.34	57.90	56.15	56.45	54.11	60.23
1395.00	55.14	52.27	58.02	55.58	59.50	51.66	1394.39	54.05	54.35	53.29	57.82	56.15	56.45	54.06	60.19
1398.00	54.92	52.02	57.81	55.37	59.22	51.52	1397.39	54.05	54.35	53.24	57.73	56.15	56.15	54.01	60.09
1401.00	54.69	51.76	57.61	55.16	58.94	51.37	1400.40	53.75	54.05	53.19	57.61	55.85	56.15	53.96	59.95
1404.00	54.47	51.51	57.43	54.95	58.68	51.22	1403.40	53.75	54.05	53.13	57.48	55.55	55.85	53.91	59.78
1407.00	54.26	51.28	57.24	54.75	58.43	51.08	1406.40	53.75	54.05	53.08	57.30	55.25	55.85	53.84	59.56
1410.00	54.06	51.07	57.04	54.57	58.18	50.96	1409.41	53.75	54.05	53.02	57.10	55.25	55.55	53.78	59.33
1413.00	53.87	50.91	56.83	54.39	57.93	50.86	1412.41	53.75	54.05	52.96	56.86	54.95	55.55	53.70	59.04
1416.00	53.70	50.79	56.61	54.24	57.66	50.82	1415.42	53.75	53.75	52.90	56.57	54.95	55.25	53.62	58.71
1419.00	53.55	50.76	56.35	54.09	57.37	50.83	1418.42	53.75	53.75	52.84	56.27	54.65	54.95	53.53	58.35
1422.00	53.41	50.75	56.07	53.98	57.06	50.89	1421.42	53.45	53.75	52.77	55.95	54.35	54.95	53.42	57.93
1425.00	53.30	50.84	55.77	53.88	56.71	51.05	1424.43	53.45	53.75	52.70	55.61	54.35	54.65	53.30	57.46
1428.00	53.22	50.98	55.45	53.81	56.32	51.29	1427.43	53.45	53.45	52.62	55.27	54.05	54.35	53.16	56.94
1431.00	53.15	51.16	55.13	53.77	55.96	51.57	1430.43	53.45	53.45	52.51	54.95	54.05	54.05	52.99	56.41
1434.00	53.10	51.32	54.87	53.75	55.65	51.85	1433.44	53.45	53.45	52.38	54.65	53.75	54.05	52.78	55.88
1437.00	53.06	51.40	54.72	53.72	55.48	51.95	1436.44	53.15	53.15	52.21	54.39	53.75	53.75	52.51	55.42
1440.00	53.03	51.38	54.68	53.69	55.40	51.98	1439.45	53.15	53.15	51.99	54.16	53.45	53.45	52.15	55.01
1443.00	53.00	51.32	54.69	53.64	55.44	51.86	1442.45	53.15	53.15	51.69	53.97	53.45	53.45	51.70	54.68
1446.00	52.98	51.15	54.81	53.57	55.47	51.66	1445.45	53.15	52.85	51.33	53.84	53.15	53.15	51.18	54.41
1449.00	52.93	50.97	54.90	53.46	55.48	51.44	1448.46	53.15	52.85	50.92	53.74	52.85	52.85	50.61	54.18
1452.00	52.86	50.78	54.94	53.33	55.45	51.22	1451.46	52.85	52.85	50.48	53.65	52.85	52.55	50.06	53.99
1455.00	52.75	50.61	54.89	53.18	55.33	51.02	1454.46	52.85	52.55	50.05	53.59	52.55	52.55	49.57	53.82
1458.00	52.62	50.43	54.81	53.00	55.18	50.81	1457.47	52.85	52.55	49.69	53.52	52.55	52.25	49.18	53.67
1461.00	52.45	50.24	54.66	52.80	54.99	50.60	1460.47	52.85	52.25	49.41	53.47	52.25	51.95	48.90	53.54
1464.00	52.														

1569.00	52.64	50.53	54.76	52.60	54.72	50.48	1568.61	53.45	53.45	51.09	55.08	53.75	53.75	50.92	54.99
1572.00	53.10	50.75	55.44	53.04	55.38	50.70	1571.61	53.75	53.75	51.17	55.99	53.75	53.75	51.15	55.42
1575.00	53.58	51.09	56.08	53.52	56.01	51.03	1574.61	53.75	53.75	51.29	56.92	53.75	54.05	51.48	56.10
1578.00	54.06	51.54	56.57	53.99	56.48	51.50	1577.62	54.05	54.05	51.48	57.23	54.05	54.05	51.98	56.64
1581.00	54.51	52.11	56.91	54.43	56.81	52.04	1580.62	54.05	54.05	51.82	57.31	54.05	54.35	52.57	56.83
1584.00	54.92	52.69	57.15	54.83	57.03	52.64	1583.63	54.05	54.35	52.53	57.28	54.35	54.35	52.90	56.87
1587.00	55.28	53.22	57.34	55.19	57.24	53.15	1586.63	54.35	54.65	52.98	57.20	54.35	54.65	53.10	56.86
1590.00	55.58	53.62	57.54	55.48	57.43	53.53	1589.63	54.65	54.65	53.15	57.16	54.65	54.65	53.23	56.86
1593.00	55.78	53.86	57.69	55.70	57.64	53.75	1592.64	54.65	54.95	53.25	57.14	54.65	54.95	53.30	56.87
1596.00	55.91	54.00	57.81	55.79	57.75	53.82	1595.64	54.95	54.95	53.31	57.11	54.95	54.95	53.37	56.86
1599.00	55.91	54.01	57.81	55.81	57.79	53.82	1598.64	55.25	55.25	53.37	57.06	54.95	54.95	53.42	56.83
1602.00	55.87	54.00	57.75	55.77	57.76	53.78	1601.65	55.25	55.25	53.42	56.97	54.95	54.95	53.47	56.76
1605.00	55.77	53.89	57.65	55.64	57.65	53.62	1604.65	55.25	55.25	53.46	56.83	54.95	54.95	53.51	56.65
1608.00	55.61	53.70	57.51	55.46	57.51	53.40	1607.66	54.95	54.95	53.49	56.66	54.95	54.95	53.52	56.51
1611.00	55.41	53.46	57.36	55.25	57.34	53.15	1610.66	54.95	54.95	53.49	56.46	54.95	54.95	53.50	56.35
1614.00	55.20	53.24	57.17	55.02	57.12	52.90	1613.66	54.65	54.65	53.45	56.25	54.65	54.65	53.42	56.16
1617.00	54.98	53.03	56.93	54.78	56.85	52.71	1616.67	54.65	54.65	53.36	56.03	54.65	54.65	53.31	55.96
1620.00	54.75	52.87	56.62	54.53	56.51	52.55	1619.67	54.35	54.35	53.22	55.82	54.35	54.35	53.16	55.76
1623.00	54.51	52.71	56.31	54.28	56.14	52.41	1622.67	54.35	54.35	53.05	55.62	54.05	54.05	52.99	55.57
1626.00	54.26	52.53	55.99	54.03	55.81	52.24	1625.68	54.05	54.05	52.87	55.44	54.05	54.05	52.80	55.39
1629.00	54.02	52.28	55.76	53.79	55.55	52.02	1628.68	53.75	53.75	52.67	55.28	53.75	53.75	52.60	55.21
1632.00	53.76	51.94	55.58	53.54	55.38	51.70	1631.69	53.45	53.75	52.46	55.13	53.45	53.45	52.39	55.04
1635.00	53.51	51.53	55.48	53.27	55.28	51.27	1634.69	53.45	53.45	52.24	55.00	53.15	53.45	52.18	54.88
1638.00	53.24	51.07	55.40	53.01	55.22	50.80	1637.69	53.15	53.15	52.01	54.86	53.15	53.15	51.96	54.71
1641.00	52.96	50.60	55.33	52.74	55.16	50.32	1640.70	52.85	52.85	51.78	54.71	52.85	52.85	51.73	54.51
1644.00	52.69	50.15	55.22	52.45	55.06	49.85	1643.70	52.55	52.55	51.54	54.52	52.55	52.55	51.50	54.29
1647.00	52.41	49.74	55.07	52.17	54.90	49.44	1646.70	52.25	52.55	51.29	54.30	52.25	52.25	51.25	54.03
1650.00	52.12	49.37	54.87	51.89	54.71	49.07	1649.71	52.25	52.25	51.04	54.05	52.25	52.25	51.01	53.77
1653.00	51.84	49.02	54.67	51.63	54.51	48.75	1652.71	51.95	51.95	50.79	53.77	51.95	51.95	50.75	53.50
1656.00	51.59	48.69	54.49	51.39	54.34	48.44	1655.72	51.65	51.65	50.52	53.48	51.65	51.65	50.50	53.21
1659.00	51.36	48.36	54.36	51.16	54.20	48.13	1658.72	51.35	51.65	50.25	53.18	51.35	51.35	50.23	52.94
1662.00	51.16	48.07	54.26	50.97	54.09	47.85	1661.72	51.35	51.35	49.97	52.88	51.35	51.35	49.96	52.66
1665.00	51.01	47.83	54.18	50.83	54.00	47.65	1664.73	51.05	51.05	49.69	52.60	51.05	51.05	49.69	52.40
1668.00	50.92	47.73	54.11	50.73	53.92	47.56	1667.73	50.75	50.75	49.42	52.32	50.75	50.75	49.43	52.14
1671.00	50.89	47.76	54.02	50.70	53.83	47.56	1670.73	50.45	50.45	49.14	52.06	50.45	50.45	49.16	51.89
1674.00	50.89	47.84	53.94	50.74	53.74	47.73	1673.74	50.45	50.45	48.86	51.80	50.45	50.45	48.89	51.65
1677.00	50.94	48.01	53.86	50.80	53.71	47.90	1676.74	50.15	50.15	48.58	51.56	50.15	50.15	48.62	51.43
1680.00	50.99	48.10	53.87	50.86	53.70	48.02	1679.75	49.85	49.85	48.31	51.33	49.85	49.85	48.35	51.21
1683.00	51.01	48.12	53.90	50.93	53.81	48.01	1682.75	49.55	49.55	48.04	51.12	49.55	49.55	48.09	51.01
1686.00	50.98	48.00	53.98	50.94	53.93	47.97	1685.75	49.55	49.25	47.76	50.93	49.55	49.25	47.81	50.81
1689.00	50.92	47.82	54.00	50.88	54.02	47.75	1688.76	49.25	49.25	47.46	50.74	49.25	49.25	47.52	50.63
1692.00	50.75	47.55	53.95	50.77	54.01	47.51	1691.76	48.95	48.95	47.14	50.54	48.95	48.95	47.21	50.43
1695.00	50.52	47.25	53.80	50.57	53.92	47.23	1694.76	48.65	48.65	46.82	50.32	48.65	48.65	46.91	50.23
1698.00	50.23	46.91	53.55	50.33	53.73	46.93	1697.77	48.35	48.35	46.49	50.10	48.65	48.35	46.59	50.02
1701.00	49.89	46.55	53.22	50.03	53.46	46.61	1700.77	48.35	48.05	46.17	49.89	48.35	48.35	46.28	49.82
1704.00	49.50	46.16	52.83	49.68	53.11	46.25	1703.78	48.05	48.05	45.83	49.69	48.05	48.05	45.96	49.62
1707.00	49.06	45.74	52.39	49.28	52.70	45.86	1706.78	47.75	47.75	45.50	49.48	47.75	47.75	45.64	49.42
1710.00	48.60	45.28	51.92	48.85	52.26	45.43	1709.78	47.45	47.45	45.16	49.26	47.75	47.45	45.31	49.21
1713.00	48.12	44.80	51.44	48.40	51.82	44.99	1712.79	47.45	47.15	44.81	49.05	47.45	47.15	44.98	49.01
1716.00	47.62	44.29	50.95	47.95	51.38	44.52	1715.79	47.15	46.85	44.46	48.84	47.15	47.15	44.65	48.80
1719.00	47.12	43.76	50.48	47.48	50.93	44.03	1718.79	46.85	46.85	44.11	48.63	46.85	46.85	44.31	48.60
1722.00	46.62	43.23	50.01	47.01	50.50	43.53	1721.80	46.55	46.55	43.76	48.42	46.85	46.55	43.98	48.39
1725.00	46.13	42.72	49.55	46.56	50.07	43.04	1724.80	46.25	46.25	43.39	48.20	46.55	46.25	43.63	48.18
1728.00	45.67	42.24	49.10	46.11	49.65	42.58	1727.81	46.25	45.95	43.03	47.99	46.25	45.95	43.28	47.98
1731.00	45.24	41.81	48.66	45.69	49.22	42.17	1730.81	45.95	45.65	42.66	47.77	45.95	45.95	42.92	47.77
1734.00	44.84	41.46	48.22	45.30	48.79	41.81	1733.81	45.65	45.35	42.24	47.56	45.95	45.65	42.53	47.57
1737.00	44.48	41.17	47.79	44.93	48.36	41.51	1736.82	45.65	45.35	41.87	47.38	45.65	45.35	42.12	47.39
1740.00	44.17	40.95	47.40	44.59	47.93	41.25	1739.82	45.35	45.05	41.68	47.20	45.35	45.05	41.82	47.21
1743.00	43.90	40.76	47.04	44.28	47.53	41.04	1742.82	45.05	44.75	41.56	47.01	45.05	44.75	41.66	47.03
1746.00	43.66	40.60	46.72	44.01	47.18	40.85	1745.83	44.75	44.45	41.47	46.83	45.05	44.75	41.56	46.85
1749.00	43.46	40.46	46.46	43.78	46.88	40.68	1748.83	44.75	44.15	41.41	46.65	44.75	44.45	41.49	46.67
1752.00	43.30	40.34	46.27	43.59	46.64	40.53	1751.84	44.45	44.15	41.37	46.47	44.45	44.15	41.43	46.49
1755.00	43.18	40.22	46.13	43.42	46.45	40.38	1754.84	44.15	43.85	41.34	46.28	44.45	43.85	41.40	46.31
1758.00	43.08	40.12	46.04	43.27	46.31	40.23	1757.84	42.05	43.55	41.33	46.10	44.15	43.85	41.39	46.13
1761.00	42.99	40.02	45.97	43.16	46.19	40.13	1760.85	42.35	43.25	41.34	45.92	42.35	43.55	41.40	45.96
1764.00	42.95	40.00	45.91	43.08	46.10	40.06	1763.85	42.35	43.25	41.36	45.74	42.35	43.25	41.40	45.78
1767.00	42.93	40.01	45.85	43.04	46.00	40.07	1766.85	42.35	42.95	41.40	45.56	42.35	42.95	41.42	45.60
1770.00	42.93	40.09	45.76	43.01	45.89	40.14	1769.86	42.35	42.65	41.44	45.39	42.35	42.95	41.46	45.43
1773.00	42.96	40.27	45.65	43.02	45.74	40.29	1772.86	42.35	42.65	41.48	45.21	42.35	42.65	41.50	45.26
1776.00	43.00	40.51	45.49	43.04	45.57	40.51	1775.87	42.65	42.65	41.53	45.04	42.65	42.65	41.54	45.09
1779.00	43.06	40.79	45.34	43.09	45.39	40.79	1778.87	42.65	42.65	41.59	44.88	42.65	42.65	41.60	44.93
1782.00	43.13	41.08	45.18	43.15	45.23	41.08	1781.87	42.65	42.65	41.65	44.72	42.65	42.65	41.66	44.77
1785.00	43.21	41.36	45.06	43.24	45.11	41.36	1784.88	42.65	42.65	41.72	44.56	42.65	42.65	41.73	44.62
1788.00	43.														